Available online at www.sciencedirect.com
ScienceDirect
Geochimica et Cosmochimica Acta 70 (2006) 5371–5394
Geochimica
www.elsevier.com/locate/gca

Brecciation and chemical heterogeneities of CI chondrites

Andreas Morlok [a,b,*], Addi Bischoff [a], Thomas Stephan [a], Christine Floss [c], Ernst Zinner [c], Elmar K. Jessberger [a]

[a] *Institut für Planetologie, Wilhelm-Klemm-Strasse 10, 48149 Münster, Germany*
[b] *Department of Earth and Planetary Sciences, Faculty of Science, Kobe University, Kobe 657-8501, Japan*
[c] *Laboratory for Space Sciences and Physics Department, Washington University, St. Louis, MO, USA*

Received 5 December 2005; accepted in revised form 3 August 2006

Abstract

Fragments in the size range from 40 μm to several hundred μm in the CI chondrites Orgueil, Ivuna, Alais, and Tonk show a wide range of chemical compositions with variations in major elements such as iron (10.4–42.4 wt% FeO), silicon (12.7–42.2 wt% SiO_2), and sulfur (1.01–15.8 wt% SO_3), but also important minor elements such as phosphorous (up to 5.2 wt% P_2O_5) or calcium (up to 6.6 wt% CaO). These variations are the result of the varying mineralogical compositions of these fragments. The distribution of phyllosilicates, magnetites, and possibly ferrihydrite, in particular, control the abundances of these elements. High REE contents—up to 150 times the solar abundances—were observed in phosphates, while matrix and sulfates are REE-depleted. The studied 113 fragments were subdivided into eight lithologies with similar mineralogical and thus chemical properties. The most common is the CGA lithology, consisting of a groundmass of Mg-rich, coarse-grained phyllosilicates and varying abundances of inclusions such as magnetite. The second most abundant lithology is the FGA lithology, consisting of a groundmass of fine-grained Fe-rich phyllosilicates. A rare, but important lithology consists of fragments with high contents of phosphates and other minerals. The proposed model for the evolution of these lithologies is based on a closed system alteration, where mineralogical differences in the lithologies reflect heterogeneities in the starting material. Comparison of our results with literature data indicates a general similarity of the four CI chondrites analyzed. Further comparison of bulk analyses suggests that the mass 'threshold' for chemical heterogeneities in CI chondrite samples is smaller than ~1–2 g.

1. Introduction

CI chondrites are considered to be chemically the most primitive rock type in the solar system, because their bulk composition is similar to that of the solar photosphere except for volatiles such as H, C, N, and O (Baars et al., 1993). Since the solar photosphere is representative for the whole sun—and comprises 99.9% of the mass of the solar system—CI chondrites are used as a proxy for the abundances of almost all elements in the solar system (Anders and Ebihara, 1982; Anders and Grevesse, 1989; Lodders, 2003). However, their chemically primitive nature does not imply that CI chondrites originated from geologically totally pristine parent bodies: of all meteorite classes CI chondrites have undergone the highest degree of alteration by fluid phases (e.g., Endreß, 1994). In addition, CI chondrites are regolith breccias (Bischoff and Schultz, 2004; Bischoff et al., 2006) formed by intense impact brecciation on their parent body. As a result, these meteorites consist of many fragments up to hundreds of μm (or larger) in size that are embedded in a fine-grained matrix (Boström and Fredriksson, 1966; Mueller and Bernal, 1966; Nagy, 1975; Richardson, 1978; Tomeoka and Buseck, 1988). In the first detailed study of fragments in CI chondrites (Orgueil, Ivuna, and Alais; Endreß, 1994), a large range of compositions was observed for major elements, and the fragments were classified into four lithologies.

A possible sequence of events on the CI chondrite parent body during the early alteration phase has already been the subject of several studies (Richardson, 1978; Tomeoka

* Corresponding author. Fax: +81 78 803 6483.
E-mail address: morlok70@kobe-u.ac.jp (A. Morlok).

0016-7037/$ - see front matter © 2006 Elsevier Inc. All rights reserved.
doi:10.1016/j.gca.2006.08.007

and Buseck, 1988; Brearley and Prinz, 1992; Buseck and Hua, 1993; Zolensky et al., 1993; Endreß, 1994; Endreß and Bischoff, 1996; Endreß et al., 1996; Brearley, 1997; Morlok et al., 2001). Here, we try to correlate these models with the chemical compositions of the fragments analyzed. The goals of the present study were to analyze a wide range of fragments with different chemical and mineralogical compositions, and to classify them into groups or lithologies. From this classification, the question of how these different types of fragments formed can be addressed.

Finally, we investigated the implications of fragmentation for the chemical homogeneity of CI chondrites. A rock used as a standard is expected to be homogeneous to allow representative analyses. If the different types of fragments are unevenly distributed in CI chondrites, this would affect the use of these meteorites as a standard for the solar system chemical composition.

2. Samples and analytical techniques

2.1. Technical methods

For the mapping of the fragments and their characterization according to the distribution of specific minerals, a scanning electron microscope (SEM) was used. For the measurement of elemental distributions, several fragments were mapped by time-of-flight secondary ion mass spectrometry (TOF-SIMS). Chemical analysis was done with an electron microprobe. All these measurements were carried out at the ICEM (Interdisciplinary Center for Electron Microscopy and Microanalysis) in Münster.

As a first step, polished thin sections were mapped in backscattered-electron mode (BSE) with a JEOL 840A (SEM). Quantitative chemical analyses were performed with a LINK AN 10000 energy dispersive X-ray spectrometer (EDX) using an accelerating voltage of 20 kV and a beam current of ~3 nA; data were corrected with the ZAF method.

Electron microprobe analyses of the fragments were made with a JEOL JXA-8600 Superprobe, using 15 kV acceleration voltage and 1.5 nA beam current. The ZAF routine was applied for the correction of matrix effects. Well-characterized natural and synthetic minerals were used as standards. The fragments were analyzed with a defocused beam (diameter 40–60 μm), and the results were averaged (for number of spots see the table in electronic annex (EA) (Table EA1). For results below detection limit, the value of the detection limit was used. For relatively heterogeneous fragments, this procedure was repeated and the mean of the two averages was taken as the representative composition.

An important point regarding the electron microbeam measurements is that a porous multi-phase system was analyzed. The high contents of water (18–22 wt%) and carbon (3–5 wt%) in CI chondrites (Brearley and Jones, 1998), as well as the high porosity of the material analyzed, resulted in low totals, generally between 70 and 80 wt% (Table EA1). Also, the measurement of a mixture of several phases (although most of them are silicates) corrected with standard matrix correction procedures affects the quality of the quantitative results. While the results are an internally consistent data set, these technical limitations should be kept in mind when the results are compared with data produced with different techniques (e.g., INAA).

To allow comparison between fragments, the results were normalized to 85.35 wt%, the sum of the analyzed elements in the solar system abundances of Anders and Grevesse (1989) recalculated as oxides (Table EA2). For comparison with literature data and statistical analysis, our data were also normalized to the silicon contents and solar system abundances (Anders and Grevesse, 1989), which have also been normalized to Si.

In the data presentation and discussion, for averages of chemical elements calculated for all fragments (and the literature data), the *geometric mean* was used. This was necessary given the wide range of compositions of the fragments, sometimes over several orders of magnitudes (P_2O_5, CaO) (Table EA1). In such cases, the values have no normal (Gaussian) distribution. The geometric mean tends to dampen the effect of very high or low values, which might bias the mean if a straight average (arithmetic mean) is calculated (Rollinson, 1993).

However, it must be emphasized that, given the wide spread of results and potential biases by sample and fragment selection, the actual range in composition is of more interest than the average concentration of an element. For this reason, we present the results in the diagrams as boxplots. Here a partitioned box shows the range of ±25% (second and third quartile) of the values around the median. The 'box' referred to in the following always means the complete box, encompassing 50% of the given results. The whisker (continuing line) extends the range to ±45%, the continuing dotted line marks the whole range of results. The average used in the boxplot diagrams is the *median*, which is the only appropriate average for this type of presentation.

Fig. 1. Secondary ion images of different species in several fragments (indicated by yellow lines), measured with TOF-SIMS in two consecutive analyses, for positive and negative secondary ions, respectively. (a) phosphate grains from fragment O12 (Orgueil), (b) images of the phosphate-rich fragment O13 (Orgueil), and a vein, filled with a Ca-rich sulfate (red arrow). (c) part of the iron-rich fragment O46 from Orgueil (bottom left) and adjacent matrix material. (d) fragment I10 (Ivuna), with a vein structure filled with sulfate (red arrow). (e) the distribution of carbonate clusters in and around fragment I9 (Ivuna). Each image has 256 × 256 pixels. Below each image the ion species is indicated. Each image is normalized to the intensity (in counts) of the most intense pixel (e.g., 47 for $^{31}P^-$), shown in red and given below the image. The color bar (top right) represents a linear scale from black (equals to zero) to red. The other number below each image represents the integrated intensity of the entire image (e.g., 1.35×10^5 for $^{31}P^-$). (For interpretation of the references to colour in this figure legend, the reader is referred to the web version of this article.)

High resolution (>0.2 μm) element distribution images were taken with an ION-TOF TOF-SIMS IV instrument (Fig. 1a–e). The primary ion beam consisted of $^{69}Ga^{+}$ ions. The sample surface was cleaned with an Ar beam prior to the analyses to remove surface contamination. Detailed information on the application of TOF-SIMS to the analysis of planetary samples can be found in Stephan (2001).

For quantitative analysis of trace elements (mainly REE) in single minerals (sulfates, phosphates) or components (matrix), the Cameca IMS-3f ion probe at

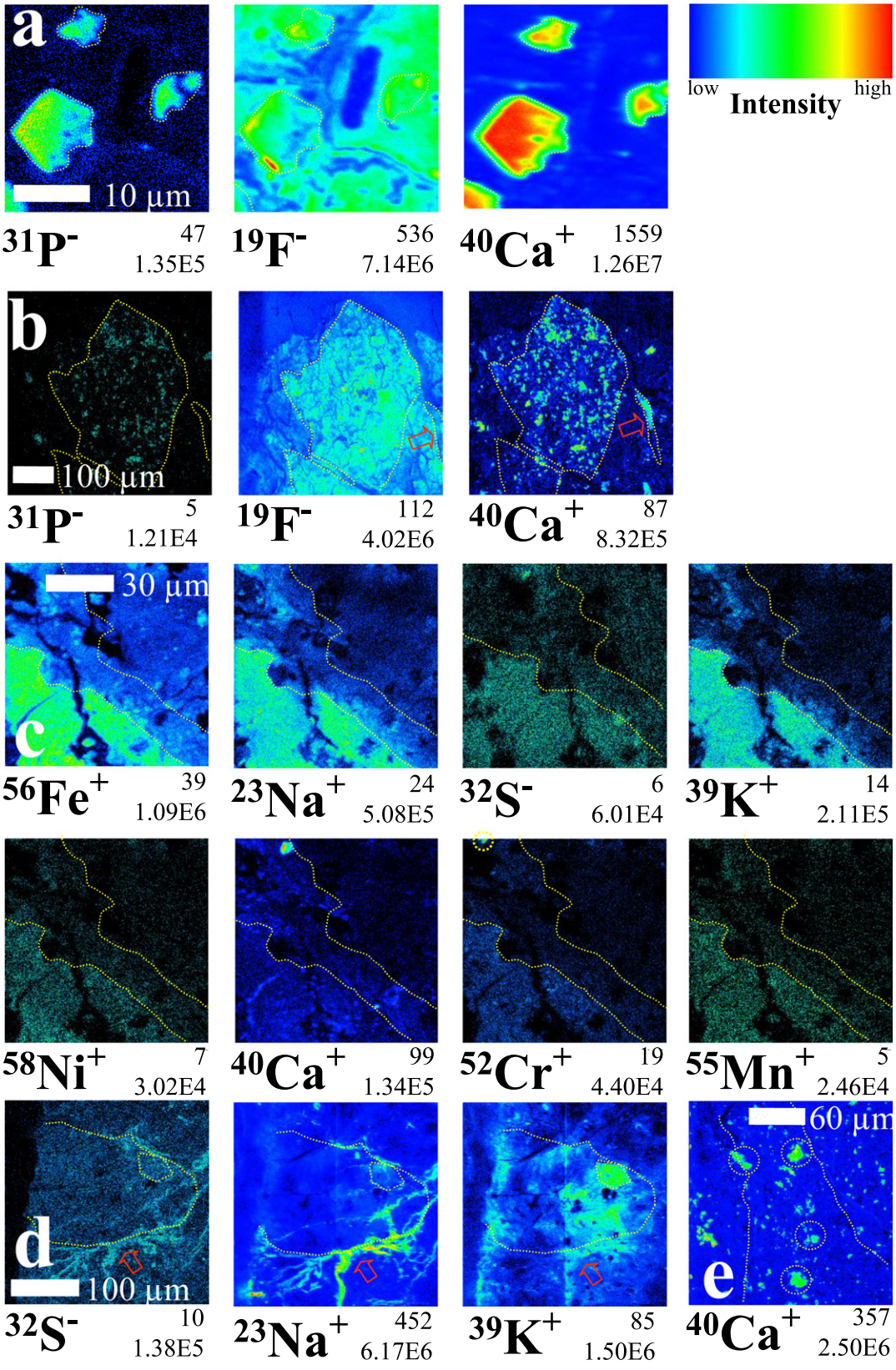

Washington University, St. Louis was used, according to techniques developed by Zinner and Crozaz (1986). The analyses were carried out using an O^- primary beam (~10 μm diameter) at low mass resolution ($m/\Delta m$ ~500). Complex interferences are removed by applying energy filtering. Simple interferences not removed by this method are corrected by deconvolution of major molecular interferences in the mass regions K–Ca–Ti, Rb–Sr–Y–Zr, and Ba-REE (Alexander, 1994). To prevent charging, the samples were coated with carbon prior to analysis. Secondary ions were collected from areas of up to 50 μm. The reference elements used to obtain quantitative trace element concentrations were Si for matrix material and Ca for sulfates and phosphates. SiO_2 and CaO concentrations of the phases analyzed were obtained by EDX analysis.

Phosphates occur mostly as clusters of small grains, rarely larger than ~20 μm, not all of which were chemically characterized with EDX or EMPA prior to the ion probe analyses. Therefore, we used the average CaO content for phosphate in CI chondrites (53.0 ± 2.1 wt%; Endreß, 1994) for quantification. Contamination from surrounding matrix material in which some of the phosphate grains were embedded occurred during the measurements of these small phases with the ion probe. Since the REE concentrations are determined by applying the REE ion yield relative to the reference element, Ca, this has an effect on the REE concentrations only if either of these elements are present in the matrix in significant quantities. Provided all Ca and REE occur in phosphates and not in the matrix, as we expect, the influence of this contamination on the REE contents of the phosphates should be insignificant. Contamination with matrix material was also encountered in the analyses of sulfates, as indicated by elevated Si contents. Similarly, measurements of the silicate-rich matrix material may have been influenced by other, smaller mineral phases that could not be avoided owing to the size of the analyzed area (Endreß, 1994).

For statistical procedures the SPSS10 software package was used. In correlation analyses the correlation coefficient r after Pearson is used. A value for r between 0.5 and 0.7 is interpreted as average, 0.7–0.9 as high and $r > 0.9$ as very high correlation (Wernecke, 1995).

For multi-variant statistical analyses, hierarchical cluster analysis with SPSS10 was applied. With this technique, it was possible to classify fragments into groups (also called clusters) with similar chemical characteristics, based on the electron microprobe data. All seven algorithms available in the software package for the calculation of clusters were used. The final eight clusters used in the study are an average of all the results. The clusters were used for the classification of the fragments into lithologies (see Section 4.2).

2.2. Samples and fragment selection

We studied samples of four of the five known CI chondrites. To document a wide range of different fragments, 14 polished thin sections were analyzed. Given the availability of material from Orgueil and the highly brecciated nature of this meteorite (e.g., Endreß, 1994), most of the fragments analyzed in this study are from this CI chondrite.

It has to be emphasized, that the focus of this study was on the composition of silicate-rich fragments, and on obtaining the composition of a wide range of such fragments as possible, and on documenting the resulting compositional diversity of CI chondrites. This easily leads to a certain bias in sampling, which is further increased by the dominance of fragments from Orgueil. When obtaining EMPA analyses of the fragments we avoided analyses of secondary minerals such as veins filled with sulfates etc., which are, by definition, not part of the fragments.

This must be kept in mind when interpreting the results, especially when comparing the averages of chemical analyses with CI (see Section 3.2).

3. Results

3.1. Description of samples

Figs. 2 and 3 and Figures EA1, 2 (EA = electronic annex) give an overview of the varying extent of fragmentation among the samples. A high degree of brecciation is exhibited by most specimens from Orgueil (Fig. 2). In this study, fragments are defined as areas that clearly distinguish themselves from the surrounding material on the basis of mineralogical and chemical composition. Fragments can show a certain degree of internal heterogeneity. However, fragments should not be confused with simple aggregates of minerals like magnetites or sulfates occurring in the matrix material.

Fig. 2 presents an enlarged image of an area in sample Orgueil 93028 and shows several typical fragments with sizes of ~100 μm embedded in a fine-grained matrix. There is no clear size range for fragments: We observed fragments larger than 1000 μm as well as small fragments that blend directly into the fine grained matrix. For technical reasons, only fragments >40 μm in size were analyzed in this study.

The fine-grained clastic matrix, which surrounds the fragments, is distinct from the groundmass within the fragments. Generally, the fine-grained clastic matrix as well as the groundmass of the fragments themselves, consists of a mixture dominated by aggregates of phyllosilicates, serpentine, and smectite, with some other minor components (Endreß, 1994). An important feature, which distinguishes the fragments, is the size of these phyllosilicate aggregates. They occur in the fragments either as so-called coarse-grained phyllosilicate aggregates (CGA) or fine-grained aggregates (FGA). The first type consists of Mg-rich material in the size range of 30–300 nm. The second group is characterized by fine-grained phyllosilicates, with crystal sizes of up to only ~30 nm. The FGA tend to be richer in iron than the CGA (Fig. 1c); they are probably finely intergrown with iron hydroxides like ferrihydrite (Kerridge, 1977; Tomeoka and Buseck, 1988; Tomeoka, 1990; Fisher and Burns, 1991; Brearley, 1992; Endreß, 1994;

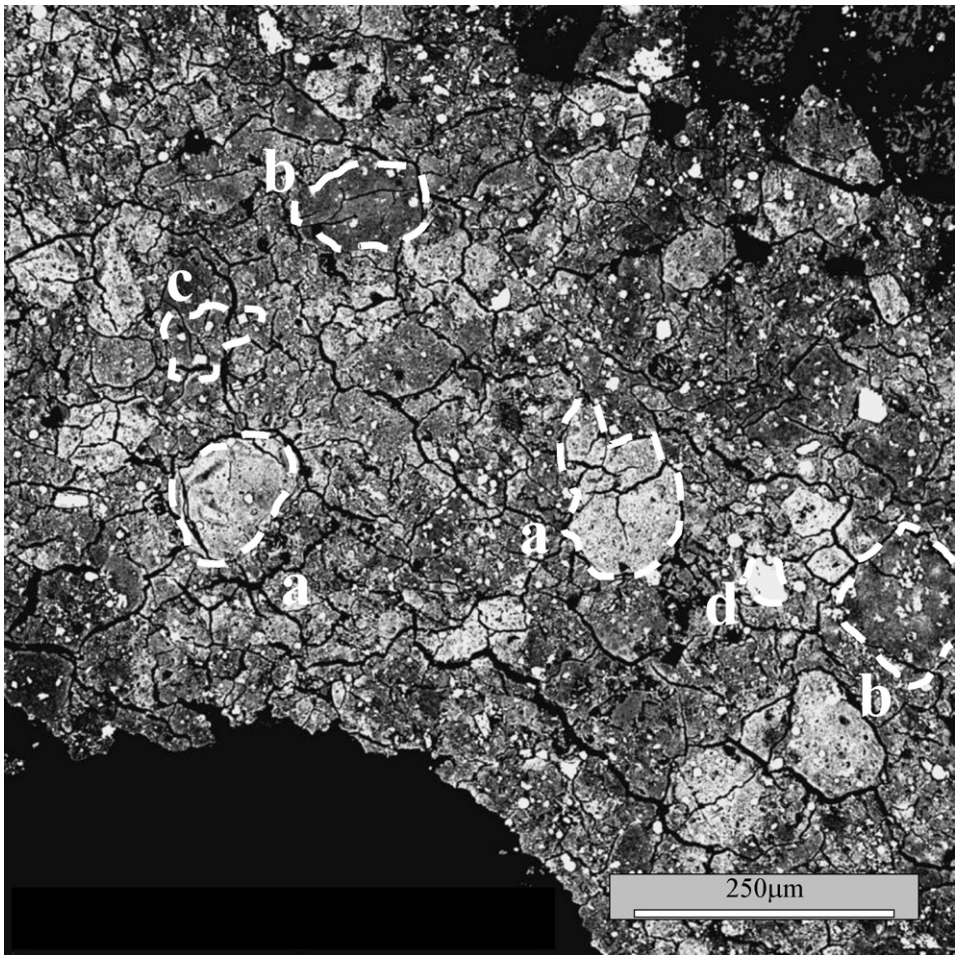

Fig. 2. BSE image of a highly brecciated area in the CI chondrite Orgueil (O93028). Fragments embedded in a fine-grained groundmass are easily visible (a–d). The groundmass differs in brightness due to varying abundance of iron. The brighter fragments (a) have higher contents in Fe than the darker ones (b). Abundant magnetites are recognizable as small, bright dots (c), similar to rare sulfides (d).

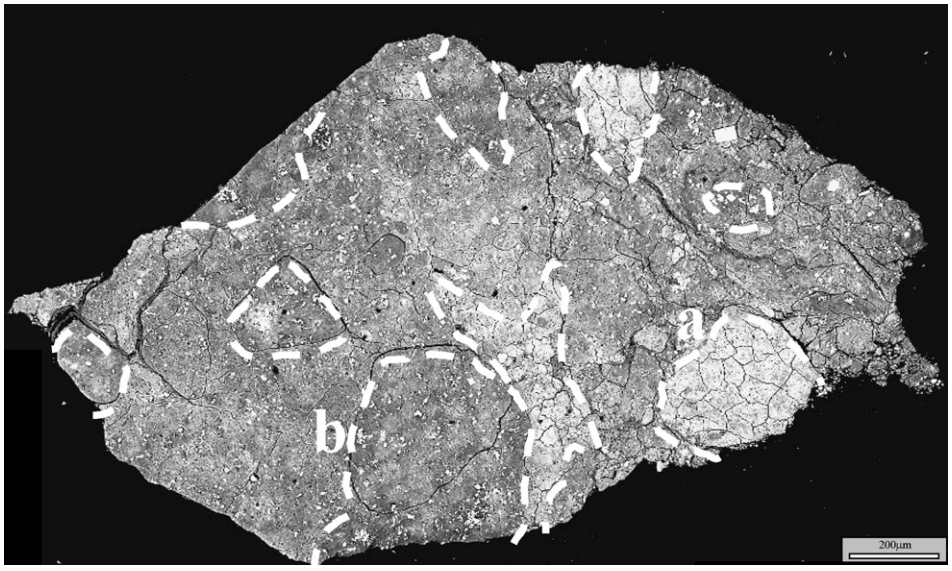

Fig. 3. BSE images of fragments in Ivuna 93161a. Three large, bright fragments are visible in the right half of the sample (e.g., a). There are also several darker fragments on the left side (e.g., b).

Bland et al., 2004). Also characteristic of CI chondrites are sulfates, recognizable as areas with high S or Ca contents which occur as secondary minerals in cracks or veins (Fig. 1b and d), and have been interpreted either as parent body or terrestrial features (Nagy, 1975; Richardson, 1978; Tomeoka and Buseck, 1988; Endreß, 1994; Gounelle and Zolensky, 2001).

Magnetites, sulfides, carbonates (Fig. 1e), and rare olivines, pyroxenes, phosphates, and other accessory minerals also occur as minor phases embedded in matrix and groundmass material in CI chondrites.

In samples from Ivuna we also found a wide variety of fragments. Ivuna 93161a (Fig. 3) has several dark, CGA-rich fragments—which are hard to distinguish from the matrix material—as well as some large FGA-rich fragments. The fragments here are relatively large, in the 200 μm range.

The samples of Alais analyzed in this study consist mainly of large fragments (or matrix areas). Alais 92322 consists of a very large CGA-rich fragment (greater than 1000 μm) with three smaller ones in the 200–400 μm range attached (Fig. EA1). Highly CGA-rich sub-fragments A13–A16, embedded in fragment A17, are possibly large phyllosilicate grains (cf. Endreß, 1994).

Fragments in Tonk are less clearly defined than in the other three CI chondrites. Tonk 94160a (Fig. EA2) has some big, CGA-rich fragments and a small FGA-rich fragment.

3.2. Chemical composition

The results of the normalized EMPA measurements of 113 fragments are presented in Table EA1 and Fig. 4a and b, which show our data and literature data normalized to CI (Anders and Grevesse, 1989) and Si.

Most elements show a wide range in concentration. In addition, the averages usually are clearly above or below CI. As pointed out above (Section 2.2), this is to be expected from the sample selection, so in the following presentation of the results the ranges are regarded as more important than the geometric means.

The SiO_2 contents of all fragments range from 12.7 wt% to 42.2 wt%. The high values of this element are due to a group of four outliers (A13, A14, A15, and A16; Table EA1) with greater than 40.0 wt% SiO_2. The bulk of the results, marked by the box, fall into the range between 27.3 wt% and 32.9 wt% SiO_2, which is above the CI abundance (22.8 wt%). The geometric mean of 29.3 wt% is also higher than the CI abundance. Silicon, aluminum, and magnesium are all positively correlated with each other and are negatively correlated with iron (Fig. 5a–c).

Most fragments are enriched in Al_2O_3 relative to CI (1.64 wt%). Here, the box is between 1.86 wt% and 2.24 wt% Al_2O_3 (Fig. 4a). The geometric mean is 2.03 wt%. Like silicon, the highest values are due to a group of outliers (A14, A15, A16; Table EA1). Apart from one fragment (O52) with a very high Al/Si-ratio ($3.36 \times$ CI), the range of ratios in our fragments is similar to those in the literature (Fig. 4b).

Like Al_2O_3 and SiO_2, most fragments have MgO contents that are higher than CI (16.4 wt%), with a geometric mean of 18.1 wt%. The box lies between 16.4 wt% and 20.1 wt% MgO (Fig. 4a). With the exception of fragment O52, which has a very high Mg/Si-ratio ($2.26 \times$ CI), the variations in Mg/Si-ratios among all fragments as well as the boxes in our study are comparable to those in the literature (Fig. 4b).

The lowest concentration of FeO is 10.4 wt% and the highest is 42.4 wt% (Table EA1). The high values are the result of two extreme outliers (O50 and O64, Table EA1); the box is between 19.9 wt% and 25.4 wt% FeO (Fig. 4a), and most measured values are below the CI value. The geometric mean of our fragments (22.3 wt%) is also slightly lower than the CI value (24.5 wt%). The highest Fe/Si-ratio ($2.77 \times$ CI) in our fragments is much higher than the literature value (0.97; Tomeoka and Buseck, 1988). Also the range of ratios is much greater than that obtained in earlier studies (Fig. 4b).

The average NiO content of the fragments (1.51 wt%) is also higher than CI (1.40 wt%), with values ranging from 0.16 wt% to 3.2 wt% (Table EA1). However, this range is largely due to two groups of outliers, one at ~3 wt% (O44, O93 and T23; Table EA1) and another below 1 wt% NiO (A13, A14, A15, and A16; Table EA1). Most results fall in the box between 1.31 wt% and 1.95 wt% NiO and most fragments are enriched in nickel compared to CI (Fig. 4a). The range and boxes of data from the literature and this study are similar (Fig. 4b).

SO_3 contents in the fragments are usually below CI, ranging from 1.01 wt% to 15.8 wt%. Most fragments have contents in the range from 6.0 wt% to 9.6 wt% SO_3 (Table EA1; Fig. 4a). The geometric mean is 7.3 wt%, about half of the CI value of 15.6 wt%; and the distribution of values among different fragments is relatively homogeneous. The high correlation with NiO ($r = 0.71$) (Fig. 5d) was also observed by Kerridge (1977). Some grains appear to lie on a separate, steeper trendline (Fig. 5d). The range of and maximum S/Si ratios are generally smaller in the literature results, with a maximum ratio of 0.76 (Tomeoka and Buseck, 1988), compared to 1.67 for Orgueil in this study.

The abundance of P_2O_5 in most fragments is below CI (Fig. 4a) and the boxplot shows 50% of the fragments to lie between 0.11 wt% and 0.3 wt% P_2O_5. The presence of a few highly enriched outliers (O12, O13, and O25; Table EA1) with up to 5.2 wt% results in a comparatively wide range of values. The geometric mean is below CI (0.19 wt% compared to 0.28 wt%). The only strong correlation is with CaO ($r = 0.74$). Maximum literature values of P_2O_5 are much lower (P/Si = $0.85 \times$ CI; Kerridge, 1976) than those in this study (25.03) (Fig. 4b).

Like P_2O_5, the CaO contents are very low among most fragments: the geometric mean is 0.25 wt%, compared with 1.3 wt% for CI, with the bulk of values ranging from 0.11 wt% to 0.59 wt% CaO, well below

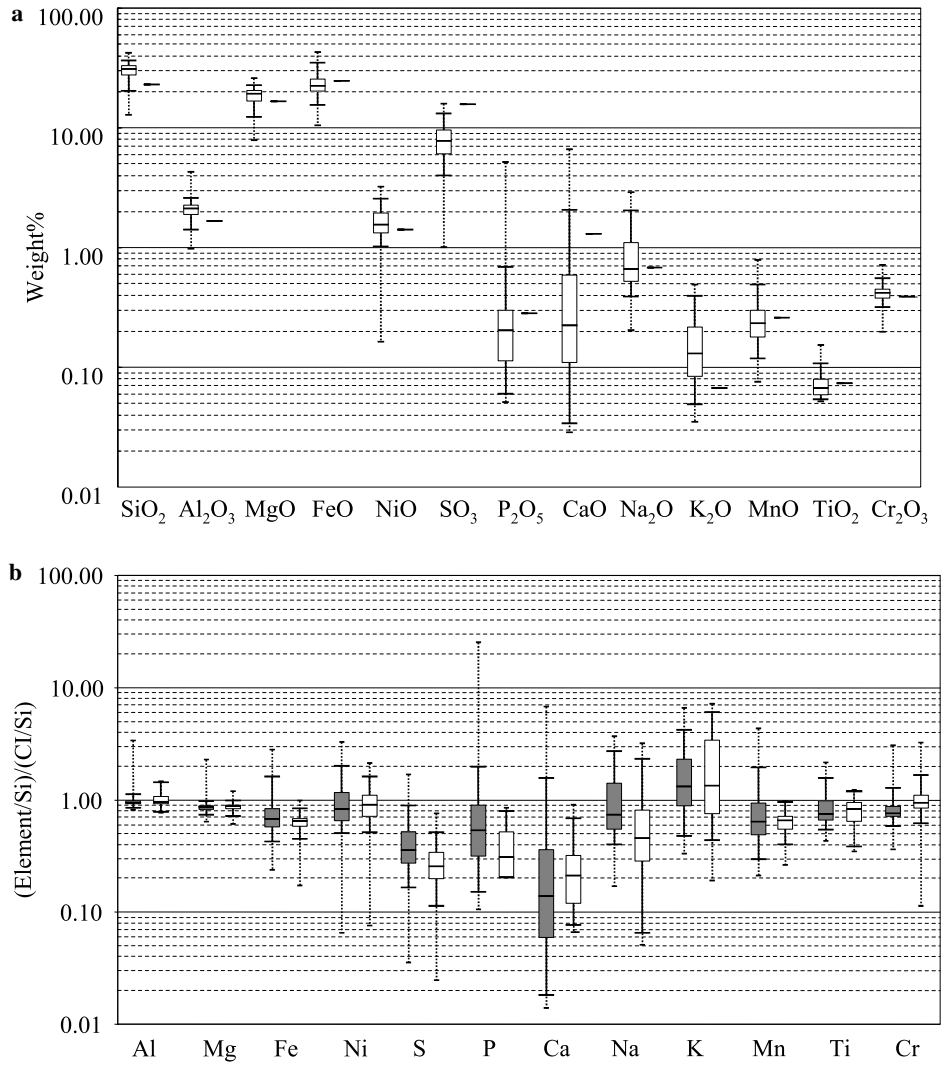

Fig. 4. (a) Boxplots of the distribution of elements in the fragments, based on the EMPA data for the 113 fragments normalized to 85.35 wt%. For results below detection limit, we used the detection limit. The whole boxes represent the second and third quartiles, encompassing ±25% of the fragments around the median. Thus, the whole box encompasses 50% of the data points of a given element. The whiskers (continuing line) extend the range to 90% of the results (±45%). The dotted lines mark the whole range of results. The symbols right to the boxplots are the solar system abundances of the given element (Anders and Grevesse, 1989). (b) EMPA analyses of major and minor elements from 113 fragments in CI chondrites (left dark boxplot), compared with literature results of matrix material and phyllosilicates (right boxplot). All data are normalized to Si and CI (represented by the horizontal line at a ratio of 1), presented in boxplots. Literature data are from Kerridge (1976), McSween and Richardson (1977), McSween (1987), Tomeoka and Buseck (1988), Zolensky et al. (1993) and Endreß (1994).

the CI value (Fig. 4a). There is a group of outliers from ~3 wt% upwards (O13, O24, and O25; Table EA1), with 6.6 wt% CaO as maximum. The highest Ca/Si ratio in our study is 6.73 × CI (Fig. 4b), much higher than literature ratios (0.90; Endreß, 1994). Also, the box is bigger than for earlier results. However, only a few fragments exceptionally enriched in CaO show such high concentrations.

The contents of Na_2O in our fragments range from 0.20 wt% to 2.86 wt% and most fragments in the box (Fig. 4a) are from 0.51 wt% to 1.1 wt% Na_2O, evenly distributed around CI (0.67 wt%). The geometric mean is 0.74 wt% (Table EA1). The literature data (Fig. 4b) show maximum values similar to those seen in our fragments with Na/Si = 3.15 × CI (McSween and Richardson, 1977) compared to 3.66 in this study (both for Orgueil).

K_2O contents range from 0.49 wt% down to 0.03 wt%, which is close to the detection limit for K_2O (0.02 wt%). Most results are in a relatively narrow box from 0.08 wt% to 0.22 wt% K_2O (Fig. 4a), enriched compared to CI. The geometric mean is 0.13 wt%, i.e., higher than CI (0.07 wt%). Maximum ratios and ranges (Fig. 4b) in the literature (K/Si = 7.09 × CI; McSween and Richardson, 1977) are comparable to those in the fragments studied here (6.54).

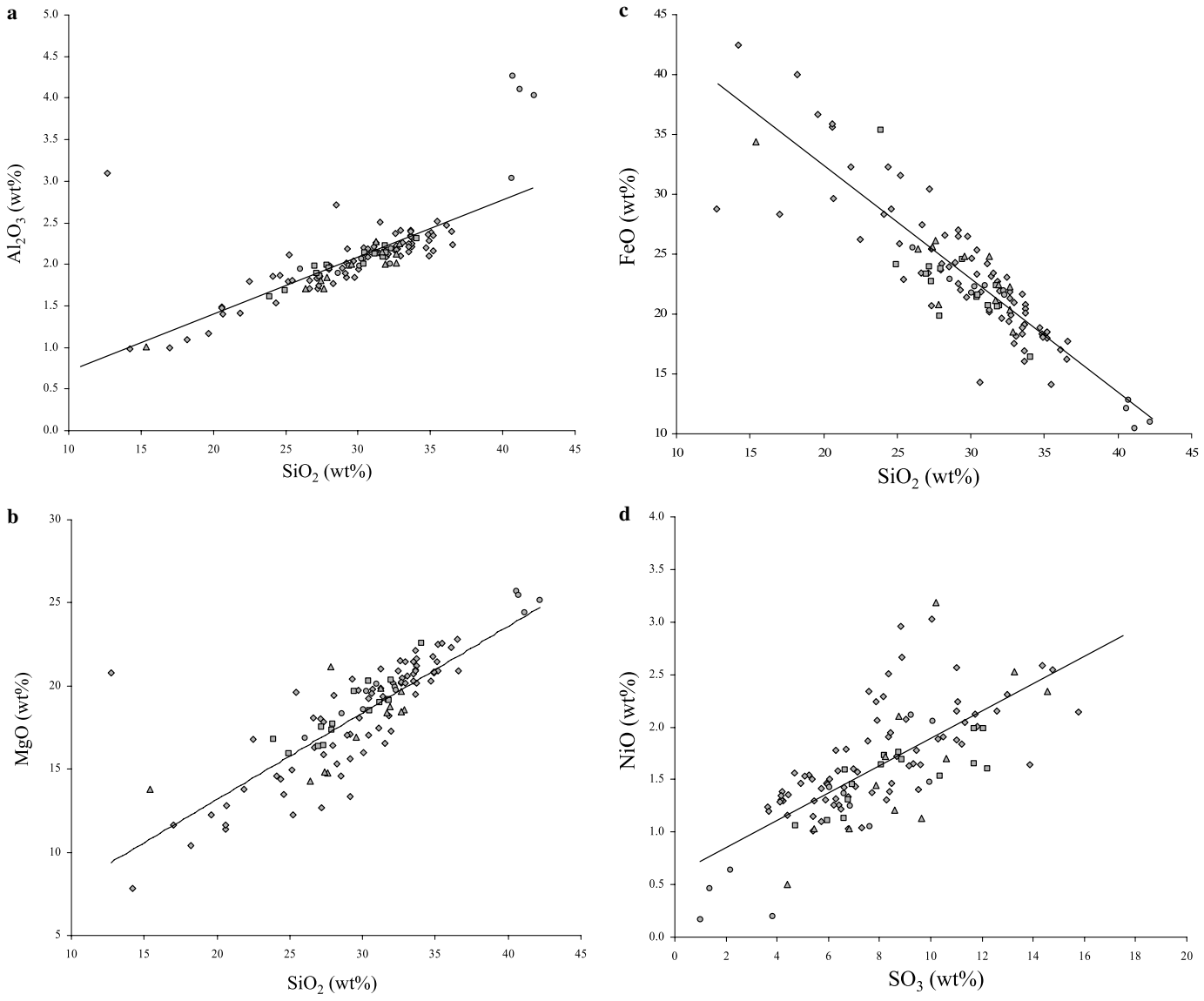

Fig. 5. (a–d) Correlation diagrams for major and minor elements in fragments from CI chondrites. EMPA data are given in wt%, normalized to 85.35 wt%. The lines are the trend lines for all fragments. Diamond (◇), Orgueil; squares (□), Ivuna; circles (○), Alais; triangles (△), Tonk.

Most of our fragments show a range of MnO (0.18–0.3 wt%) concentrations, evenly spread around CI (0.26 wt%) (Fig. 4a). The geometric mean of the fragments (0.23 wt%) and CI (0.26 wt%) are very close. The maximum Mn/Si ratio reported in the literature (0.96 × CI; Zolensky et al., 1993) is much lower than that obtained here (4.32) (Fig. 4b).

The geometric mean of TiO_2 among the fragments (0.07 wt%) is very close to the detection limit of 0.05 wt%, and identical to CI (0.07 wt%) (Table EA1). Concentrations of Cr_2O_3 in fragments range from 0.20 wt% to 0.71 wt% (Table EA1), with the bulk lying between 0.37 wt% and 0.45 wt% (Fig. 4a), evenly distributed around CI (0.39 wt%). Maximum Cr/Si ratios (3.04 × CI) are similar to literature values (3.23 × CI) (Fig. 4b).

3.3. TOF-SIMS analyses

Element distribution images obtained with TOF-SIMS give insights into the spatial distribution of major and minor elements between and inside the fragments. The high-resolution images were especially helpful for mapping different phases in the phosphate rich fragments (Fig. 1a and b). In addition, chemical differences between the main lithologies are shown in a direct comparison of a FSA and a GSA rich fragment in Fig. 1c. The effects of aqueous alteration such as leaching of elements from a fragment into sulfate (see Section 4), is shown in Fig. 1d.

Phosphate cluster in fragment O12: The distribution of P, F, and Ca in a cluster of typical, fine-grained phosphate grains with a size of 10 μm and smaller is shown in Fig. 1a. Calcium and phosphate are concentrated only in

the phosphates, while fluorine also occurs in the surrounding material.

Phosphate-rich fragment O13: An example of a fragment consisting of many phosphate clusters, as in Fig. 1a, is shown. The groundmass of the whole fragment is enriched in fluorine compared to the surrounding matrix. Calcium also occurs in other phases (probable carbonates and sulfates) besides phosphates, both inside the fragment and as some larger grains in the surrounding matrix. Calcium is also enriched in a typical sulfate, filling part of a crack (see red arrow).

Fine-grained, iron-rich fragment O46: Two types of fragments with very pronounced differences in composition, separated by dotted, yellow lines, can be observed in Fig. 1c. An iron-rich fragment (O46) that is also enriched in Na, S, K, Ni, Ca, Cr, and Mn in its groundmass can be seen in the lower left of the image. The elements are distributed very homogeneously, without 'hotspots' due to larger mineral grains. Another, iron-poor fragment is in the upper right part of the image. Both fragments are divided by a diagonal strip of matrix material.

Sulfate vein and fragment I10: Fig. 1d shows a crack filled with a sodium and potassium-rich sulfate (red arrow). Above this structure, the iron-rich fragment I10, similar to that in Fig. 1c, also exhibits a clear enrichment in potassium.

Carbonate-aggregates in Fragment I9 (Fig. 1e): Clusters of carbonates are presented in Fig. 1e. Here these minerals occur inside of fine-grained, iron-rich fragment I9.

3.4. REE analyses

Matrix areas: The REE abundances in the matrix lie close to or below CI (Fig. 6a, and Table 1a). The lowest value is $0.15 \times$ CI for europium in M2, a CGA-rich area. The highest REE abundances were found in M7, a FGA-rich area with $1.02 \times$ CI (only for Pr). The patterns of most matrix analyses are relatively flat within errors. Negative europium anomalies were found in M2 and M9. However, due to the large error bars, especially for low abundances, not all variations in the patterns may be significant.

Sulfates: REE contents in sulfates range up to $3.7 \times$ CI for Tm in S3 (Fig. 6b, Table 1b). S11 and S14 are the purest sulfate samples with little contamination by matrix material; they are depleted in REE compared to CI, and the light

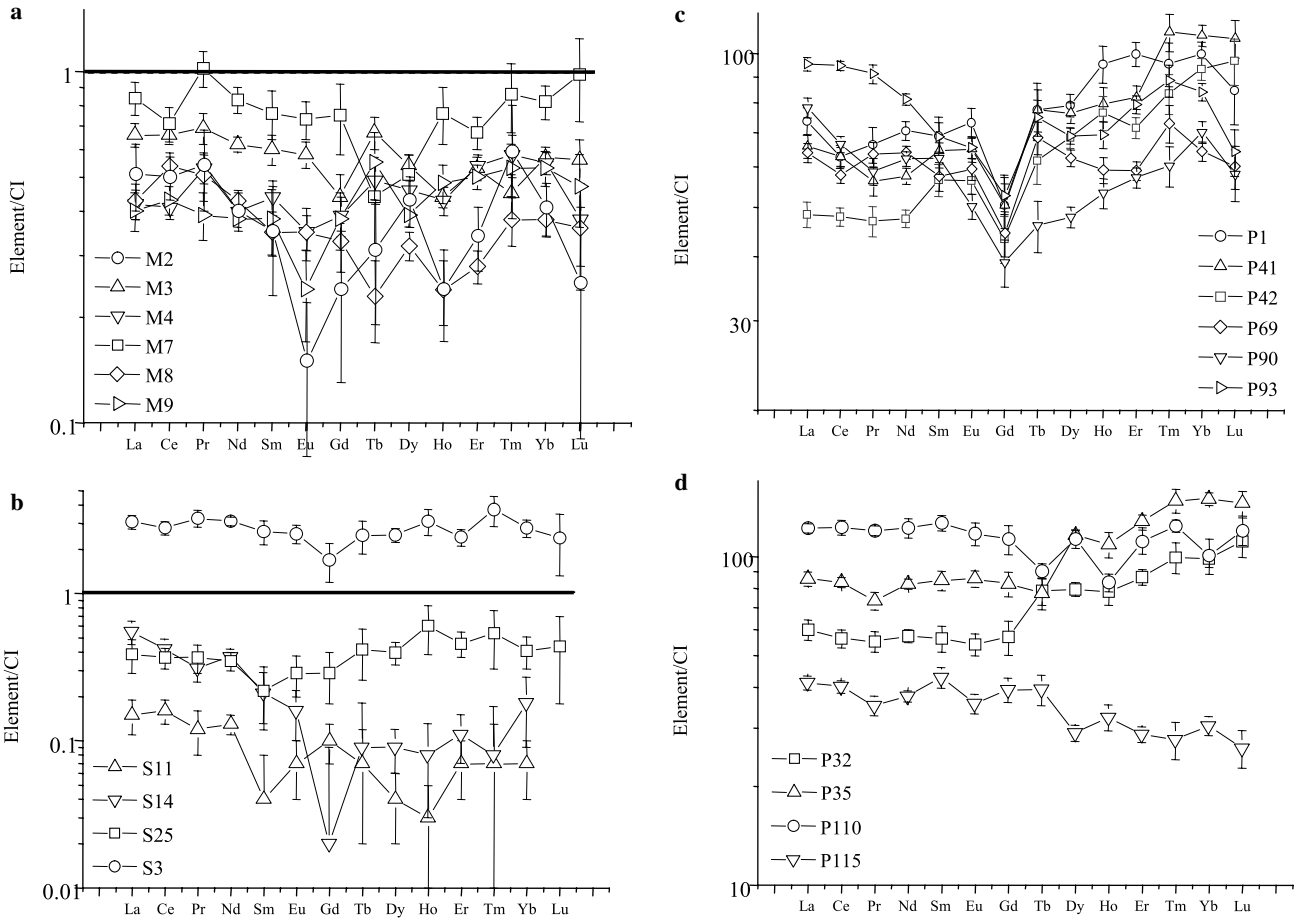

Fig. 6. (a–d) CI chondrite-normalized REE patterns in phases from CI chondrites. (a) REE abundances in matrix areas from CI chondrites are usually depleted compared to CI, as are the sulfates (b). One sulfate grain (S3) shows an enrichment of ~2–3 × CI. (c) and (d) REE contents in phosphate grains from Orgueil are distinctly enriched over CI abundances. Characteristic for some analyses of this phase is a negative Gd anomaly (c). A few phosphate grains from Orgueil (P32, P35) have heavy REE enriched relative to the light REE. P110 and 115 have comparatively flat REE patterns (d).

Table 1
(a–c): REE contents (in ppm) in matrix (a), sulfates (b) and phosphates (c) from CI chondrites (c)

	M2	M3	M4	M7	M8	M9
(*a*)						
La	0.12 ± 0.02	0.15 ± 0.01	0.1 ± 0.01	0.2 ± 0.02	0.1 ± 0.01	0.09 ± 0.01
Ce	0.3 ± 0.04	0.4	0.25	0.43 ± 0.05	0.33	0.26
Pr	0.05 ± 0.01	0.06 ± 0.01	0.05	0.09 ± 0.01	0.05 ± 0.01	0.03 ± 0.01
Nd	0.18 ± 0.02	0.28	0.18	0.38	0.19	0.17
Sm	0.05 ± 0.02	0.09 ± 0.01	0.07 ± 0.01	0.11 ± 0.02	0.05 ± 0.01	0.06 ± 0.01
Eu	0.01	0.03	0.02	0.04	0.02	0.01
Gd	0.05 ± 0.02	0.09 ± 0.01	0.08 ± 0.01	0.15 ± 0.03	0.06 ± 0.01	0.07 ± 0.01
Tb	0.01	0.02	0.02	0.02	0.01	0.02
Dy	0.1 ± 0.02	0.13	0.11	0.12 ± 0.02	0.08 ± 0.01	0.09 ± 0.01
Ho	0.01	0.02	0.02	0.04 ± 0.01	0.01	0.03
Er	0.05 ± 0.01	0.08 ± 0.01	0.09 ± 0.01	0.11	0.04	0.08 ± 0.01
Tm	0.01	0.01	0.01	0.02	0.01	0.01
Yb	0.07 ± 0.01	0.09 ± 0.01	0.09 ± 0.01	0.13 ± 0.02	0.06 ± 0.01	0.09 ± 0.01
Lu	0.01	0.01	0.01	0.02 ± 0.01	0.01	0.01
	S2	S3	S11	S14	S21	S25
(*b*)						
La	0.15 ± 0.02	0.72 ± 0.08	0.04 ± 0.01	0.13 ± 0.02	0.1 ± 0.02	0.09 ± 0.02
Ce	0.47	1.69 ± 0.17	0.1 ± 0.02	0.25 ± 0.04	0.14 ± 0.03	0.22 ± 0.04
Pr	0.05 ± 0.01	0.29 ± 0.04	0.01	0.03 ± 0.01	0.03 ± 0.01	0.03 ± 0.01
Nd	0.36	1.41	0.06 ± 0.01	0.17 ± 0.02	0.16 ± 0.02	0.16 ± 0.02
Sm	0.09 ± 0.03	0.39 ± 0.07	0.01 ± 0.01	0.03 ± 0.01	0.01 ± 0.01	0.03 ± 0.01
Eu	0.02 ± 0.01	0.14 ± 0.02	n.d.	0.01	0.01	0.02 ± 0.01
Gd	0.11 ± 0.03	0.33 ± 0.1	0.02 ± 0.01	n.d.	0.04 ± 0.01	0.06 ± 0.02
Tb	0.03	0.09 ± 0.02	n.d.	n.d.	0.01	0.02 ± 0.01
Dy	0.15 ± 0.02	0.61 ± 0.07	0.01	0.02 ± 0.01	0.06 ± 0.01	0.1 ± 0.02
Ho	0.04 ± 0.01	0.17 ± 0.03	n.d.	n.d.	0.01	0.03 ± 0.01
Er	0.13 ± 0.02	0.39 ± 0.05	0.01	0.02 ± 0.01	0.02 ± 0.01	0.07 ± 0.01
Tm	0.02 ± 0.01	0.09 ± 0.02	n.d.	n.d.	n.d.	0.01 ± 0.01
Yb	0.16	0.45 ± 0.06	0.01 ± 0.01	0.03 ± 0.01	0.04 ± 0.01	0.07 ± 0.02
Lu	0.02 ± 0.01	0.06 ± 0.03	n.d.	n.d.	n.d.	0.01 ± 0.01

	P1	P2	P35	P41	P42	P69	P90	P93	P110	P115
(*c*)										
La	17.3	14	20.1	15.4	11.4	15	18.4	22.4	28.5	9.7
Ce	37.9	33.9	50.3	37.9	29	34.9	40	57.1	73.7	24.2
Pr	5.9	4.9	6.5	5	4.2	5.7	5.2	8.1	10.6	3.1
Nd	31.9	25.9	37.3	26	21.5	29	28.1	36.8	55	17
Sm	10.1	8.3	12.4	9.5	8.3	8.5	9.2	10.1	18.5	6.3
Eu	4.1	3	4.8	3.6	3.2	3.3	2.8	3.7	6.5	2
Gd	9.9 ± 1.45	11.2 ± 1.32	16.2	9.9 ± 1	8.5 ± 0.91	8.8 ± 0.89	7.7 ± 0.81	10.4	22.1	7.7
Tb	2.8 ± 0.36	2.9	2.8 ± 0.3	2.8	2.2 ± 0.23	2.5	1.7 ± 0.19	2.7	3.3 ± 0.41	1.4 ± 0.15
Dy	19.2	19.3	28.2	18.6	16.6	15.2	11.6	16.7	27.3	7
Ho	5.3	4.3	6.1	4.4	4.3	3.3	3	3.9	4.6	1.8
Er	15.8	13.7	20.4	13	11.4	9.4	9.1	12.6	17.6	4.6
Tm	2.3 ± 0.23	2.4 ± 0.26	3.6	2.7	2	1.8	1.5	2.1	3	0.7 ± 0.09
Yb	16.2	16	24.3	17.6	15.2	10.5	11.4	13.7	16.3	5
Lu	2.1 ± 0.3	2.7 ± 0.28	3.5	2.6	2.4 ± 0.25	1.5	1.4 ± 0.16	1.6 ± 0.16	2.9 ± 0.29	0.6 ± 0.08

Absolute errors (1σ) are only presented when larger than 10% of the concentration.
n.d., not detected.

REE (LREE) are enriched relative to the heavy REE (HREE). The patterns for S25 and S3 are relatively flat; S3 shows a small negative Gd anomaly, S25 has slightly enriched HREE. This could be the result of contamination with a phosphate (see below), although the chemical analysis of this area shows no enrichment in P.

Phosphates: Phosphates have REE abundances ranging from 26 × CI for Lu (P115) to 150 × CI for Yb (P35; Fig. 6c, d and Table 1c). Most abundances are in the ~70 × CI range for the LREE and ~90 × CI for the HREE. Phosphates exhibit a variety of patterns: several of the grains (P1, P41, P42, P69, P90, P93) have distinct negative Gd anomalies (Fig. 6c), while others have enriched HREE contents compared with those of the LREE (P1, P32, P35, P41, P42; Fig. 6d). Some patterns (P41, P42) show both features.

4. Discussion

4.1. Chemical heterogeneity and mineralogical diversity

Matrix material/phyllosilicates and SiO_2, MgO, and Al_2O_3: Silicon, aluminum, and magnesium are all positively correlated with each other and are negatively correlated with iron (Fig. 5a–c). The high correlation coefficients between SiO_2, MgO and Al_2O_3 ($r > 0.7$) indicate that the distribution of these elements is mainly controlled by the abundance of phyllosilicates, which are the dominant phase in CI chondrites (50.0–71.5 wt%; (Boström and Fredriksson, 1966; Kerridge, 1967; Bland et al., 2004). The types of phyllosilicates known to be present in Orgueil, Ivuna, and Alais are Mg-rich serpentinite and smectite/saponite (MacKinnon and Kaser, 1988; Tomeoka and Buseck, 1988; Tomeoka, 1990; Brearley, 1992; Bland et al., 2004).

A ternary diagram of Fe, Mg and Si + Al helps to estimate the amounts of serpentine and smectite in the fragments (Tomeoka and Buseck, 1988) (Fig. 7). Most fragments cluster around a line for the solid solution of serpentine ($(Mg, Fe)_6(Si, Al)_4O_{10}(OH)_8$), with the bulk of

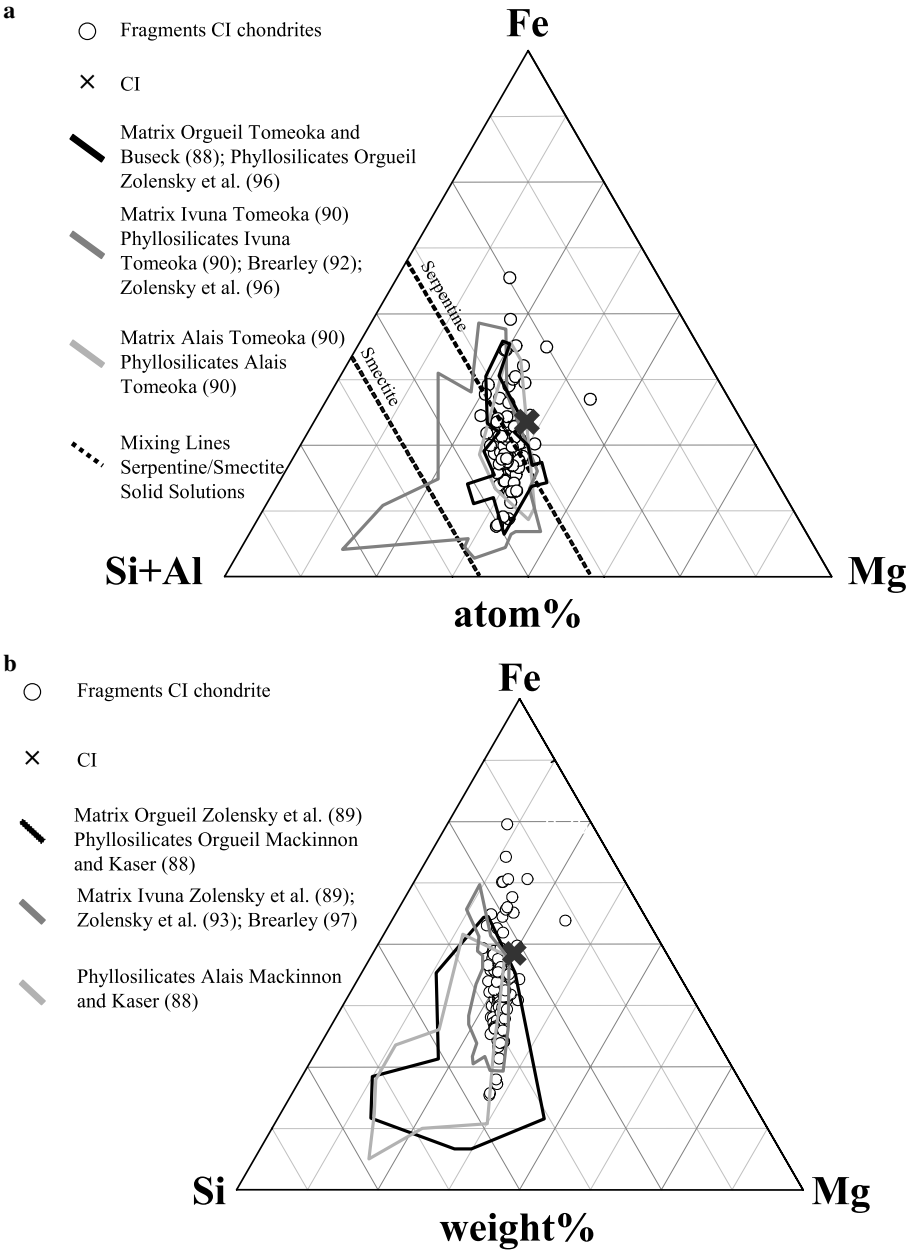

Fig. 7. (a, b) Ternary diagrams of Fe, Si, Mg in fragments from CI chondrites in atom% (a) and weight% (b). The thick unbroken lines mark the areas covered by matrix and phyllosilicate analyses compiled from earlier studies. The broken lines in (a) mark the solid solution lines for serpentine and smectite. The literature data of (a) and (b) from different CI chondrites (Orgueil, Ivuna, Alais) cover similar areas, Given the dominance of matrix material in the fragments, this indicates a general similarity in the distribution of lithologies among the various CI chondrites. (See above-mentioned references for further information.)

fragments falling in the area between the serpentine and smectite ($(Mg, Fe)_3(Si, Al)_4O_{10}(OH)_2$) solid solution lines. However, not all iron occurs in the phyllosilicates, as the fragments usually also contain inclusions such as magnetite or sulfides (see below). This makes an exact mineralogical interpretation (especially of the serpentine/smectite ratio) of the diagram difficult. While fragments are dominated by phyllosilicates, the inclusions will influence the chemical composition. It can be assumed that without the additional iron from the inclusions, all fragments would fall between the two phyllosilicates solid solution lines.

Literature data of matrix and phyllosilicates from Orgueil, Ivuna, and Alais fall into similar areas (Fig. 7a and b).

A comparison of the combined literature data with the results of this study shows that our results mostly overlap with the literature data, with the exception of some fragments with high iron content. However, the area covered by the fragments is much smaller and narrower than that of the literature data, probably the result of the integration of a larger area in the defocused beam analyses.

Magnetite/Ferrihydrite and FeO: Magnetite, with an abundance of 6–17 wt% in CI chondrites (Boström and Fredriksson, 1966; Kerridge, 1967; Bland et al., 2004) is one of the minerals with the strongest impact on the iron contents of the fragments. As the images of samples and fragments show, this mineral is unevenly distributed in CI chondrites and occurs both in the form of big grains and as abundant, small particles with sizes less than 1 μm.

Compositional variations of fragments in the ternary diagrams (Fig. 7a and b) suggest another important carrier of Fe. Most analyses lie on a straight line, which is the result of varying iron content, while the variations of Si, Al, and Mg are less pronounced. There is a moderate correlation of Fe with Ni and S, and a high anticorrelation with SiO_2 ($r = -0.88$; Fig. 5c). Similar correlations were interpreted by Tomeoka and Buseck (1988) as indicators for the occurrence of ferrihydrite in CI chondrites. According to their work, ~60% of iron in matrix material and ~34% in bulk CI chondrites occurs as iron hydroxide, which probably is closely intergrown with the phyllosilicates. Analyses of FGA show high (up to 29.5 wt%) contents of iron in this material (Endreß, 1994). Elemental distribution images also show that iron is often homogeneously distributed in the groundmass of the fragments (Fig. 1c). Ferrihydrite is known to absorb other elements into its structure (Tomeoka and Buseck, 1988), and could influence the compositions of the fragments. The TOF-SIMS distribution images (e.g., Fig. 1c) indicate a correlation of Na, S, K, Ni, Ca, Cr, and Mn with the fine-grained, iron-rich matrix. However, of these elements only S and Mn show a reasonable positive correlation with Fe ($r = 0.6$ and 0.59, respectively) when the EMPA data are used. The occurrence of ferrihydrite in all CI chondrites is contested, although most workers agree on its occurrence in Orgueil (e.g., Tomeoka and Buseck, 1988; Tomeoka, 1990; Brearley, 1992; Bland et al., 2004). Tomeoka and Buseck (1988), and Bland et al. (2004) measured 5 wt% of ferrihydrite in Orgueil. There are indications for its occurrence in Alais and Ivuna (Tomeoka, 1990; Fisher and Burns, 1991); however, Brearley (1992) and Endreß (1994) found no evidence for this phase in Alais, Ivuna, and Tonk. Zolensky et al. (1993) report only small amounts of ferrihydrite in Ivuna. The fact that fragments from the four CI chondrites measured in this study all plot on a straight line in the ternary diagrams (Fig. 7a and b) could indicate the occurrence of ferrihydrite in all these meteorites, according to the argument of Tomeoka and Buseck (1988).

The reason for this incoherent picture regarding the occurrence of ferrihydrite is not entirely clear. The techniques used by most groups are similar—transmission electron microscopy and electron microprobe analysis (Tomeoka and Buseck, 1988; Tomeoka, 1990; Brearley, 1992; Zolensky et al., 1993; Endreß, 1994), thus differences in analysis techniques do not explain the differences. Mössbauer spectroscopy, which allows a direct determination of ferrihydrite, has only been used on Orgueil so far (Wdowiak and Agresti, 1984; Madsen et al., 1986; Fisher and Burns, 1991; Bland et al., 2004).

One reason for these discrepancies could be the heterogeneity of fragments with different compositions, as discussed in this paper. Some workers attribute the occurrence of ferrihydrite to varying degrees of aqueous alteration (e.g., Brearley, 1997), therefore an uneven oxidation of the materials could play a role here. In addition, terrestrial alteration cannot be completely ruled out.

Sulfates and S, Ca, Ni, Na, K: With the exception of a few fragments, sulfur is depleted in the fragments compared to CI (Fig. 4a). The reason for this is that up to 74 wt% of sulfur in CI chondrites occurs in sulfates (Burgess et al., 1991), which contain 29.9 to 59.7 wt% SO_3 (Endreß, 1994). Distribution maps for sulfur and other elements (Fig. 1d) show the occurrence of sulfates as fillings of cracks and veins. Because of this, S, Ca, Ni, and Na are probably leached out of the fragments, thus lowering the median concentrations of these elements below CI. Potassium, however is not depleted relative to CI, pointing to the role of other phases (e.g., ferrihydrite).

Elements affected by the uneven distribution of sulfates may include calcium (up to 39.7 wt% CaO in sulfates), nickel (up to 12.3 wt%), potassium (up to 15.6 wt%) and sodium (up to 0.99 wt%; Endreß, 1994). However, the correlation of the latter three elements with sulfur is not high, since these elements also occur in other important phases. On the other hand, the distribution of Na-rich and K-rich fragments (Fig. EA3) is very similar to the distribution of sulfate compositions in CI chondrites (Endreß, 1994). Tomeoka and Buseck (1988) postulated the adsorption of sulfates onto ferrihydrite. This could explain the enrichment of sulfur, sodium, and potassium in the groundmass of FGA fragments (Fig. 1c). Sulfur exhibits a moderate ($r = 0.6$) correlation with iron.

Carbonates and Ca, Mn: With abundances of up to 2.8 wt%, carbonates are one of the common components

in CI chondrites (Boström and Fredriksson, 1966; Endreß and Bischoff, 1996). Carbonates in CI chondrites have CaO concentrations up to 57.6 wt% (Endreß, 1994). These carbonate grains, which can have sizes of several hundred micrometer (Nagy, 1975; Endreß, 1994), are unevenly distributed and occur mainly outside of fragments. There seem to be only a few fragments with high carbonate abundances of up to 35 vol% (compare Fig. 1e), as observed by Fredriksson and Kerridge (1988).

Carbonates have Mn abundances of up to 12 wt%, and are the main carrier of this element in CI chondrites (Endreß, 1994). The scarcity of carbonates in fragments probably explains the low Mn contents among the fragments (Fig. 4a and b).

Sulfides and S, Fe, Ni: Fe–Ni sulfides are among the prevalent mineral phases in CI chondrites (4.6 to 6.3 wt%; Boström and Fredriksson, 1966; Kerridge, 1967; Bland et al., 2004). The distribution of nickel appears to be strongly controlled by pyrrhotite (0.35–3.4 wt% Ni) and pentlandite (9.2–27.4 wt% Ni; Endreß, 1994; Bullock et al., 2005).

Phosphates and P, Ca, REE, Na, Ni: The main carrier of phosphorous in CI chondrites is Ca-rich phosphate (Fig. 1a and b), probably apatite with 36.2–44.5 wt% P_2O_5 (Endreß, 1994). Since phosphates are concentrated in few fragments, phosphorous and some other elements that mainly occur in phosphates, are unevenly distributed in CI chondrites. CaO is highly correlated with P_2O_5 ($r = 0.75$), with contents of up to 56.0 wt% (Endreß, 1994). In some cases phosphates can have high abundances of Na_2O (up to 2.55 wt%) and MnO (up to 1.24 wt%; Endreß, 1994). Phosphates also basically control the REE abundances in CI chondrites.

REE: A notable feature of the REE patterns of some of the phosphates is the presence of negative Gd anomalies. Such anomalies have previously been found only in some phosphates from H chondrites (Crozaz et al., 1989). Evensen et al. (1978) reported 13 positive and 2 negative Gd anomalies in bulk analyses of several meteorites. However, the positive anomalies were attributed to technical problems. More recently, positive Gd anomalies were found to occur in fine-grained rims around components in CM chondrites (Hua et al., 2002). It has been suggested that Gd hydroxide (as either the $Gd(OH)^{2+}$ or $Gd(H_2O)_x^{3+}$ species) is more stable than hydroxides of the other REE (Brookins, 1989). Thus, one possibility is that Gd preferentially remained in solution during formation of the phosphates through aqueous alteration of CI chondrites. However, this fractionation mechanism is controversial (Brookins, 1989) and cannot explain the existence of similar Gd anomalies in phosphates from H chondrites (Crozaz et al., 1989).

Accessory minerals: Several rare mineral phases with high contents of specific elements also influence the elemental composition of CI chondrites despite their scarcity. Ilmenite in CI chondrites contains up to 11.7 wt% MnO and 55.7 wt% TiO_2. Furthermore, high abundances of minor elements can be found in spinels: up to 54.5 wt% Cr_2O_3 and 2.61 wt% TiO_2. An unidentified, so-called 'K-rich phase' with up to 6.3 wt% K_2O and 6.5 wt% Na_2O has also been observed (Endreß, 1994). Finally, some sulfur occurs as atomic sulfur in organic components (Burgess et al., 1991).

4.2. Formation of the fragments

The mineralogy of CI chondrites is the result of extensive alteration on the parent body. This alteration occurred in several steps, with characteristic changes in mineralogy (e.g., Tomeoka and Buseck, 1988; Endreß and Bischoff, 1996). As a consequence, the wide range in chemical composition results from the changing mineralogy of the fragments due to these episodes of parent body alteration. In the following, we evaluate whether the different types of fragments give additional insights into the alteration process, and help to confirm those earlier models.

It is convenient to classify the variety of fragments into groups with similar chemical and mineralogical characteristics. This makes it easier to relate the fragments to individual steps in models of CI parent body alteration, with their characteristic mineralogies (e.g., Tomeoka and Buseck, 1988; Endreß and Bischoff, 1996). Endreß (1994) and Endreß and Bischoff (1994) identified several lithologies in the CI chondrite Ivuna. Here we classify the fragments found into additional lithologies (Fig. 8).

It is, of course, not possible to determine whether fragments of the same lithology formed from the same precursor at the same time on the parent body, or if they comprise material from different sources that were affected by similar processes (see Section 4 below).

4.2.1. Lithologies in CI chondrites

We used simple mineralogical criteria for the classification, based on BSE and TOF-SIMS images. The mineralogical composition of the groundmass was the first criteria: Does it consist of fine-grained, iron-rich FGA material or coarse clusters of magnesium-rich CGA material? From this, the two major lithologies, FGA and CGA, were defined. The second criterion was the occurrence and type of mineral inclusions inside the groundmass.

Any classification based on BSE images can be ambiguous in some cases. This was especially the case for fragments with many inclusions, where the type of groundmass was difficult to determine (e.g., the iron-rich end member of the CGA lithology).

As an additional means for characterization, we used hierarchical cluster analysis to classify the fragments into groups or clusters with specific chemical characteristics.

However, since the clusters are entirely based on the chemistry of the fragments, a CGA-rich fragment with many inclusions could, e.g., yield a bulk chemistry like a FGA fragment, thus ending up in the same cluster. Still, the clusters provide a convenient means of subdividing the lithologies into smaller units. Within the context of the lithologies as presented in Fig. 8, the vertical divisions

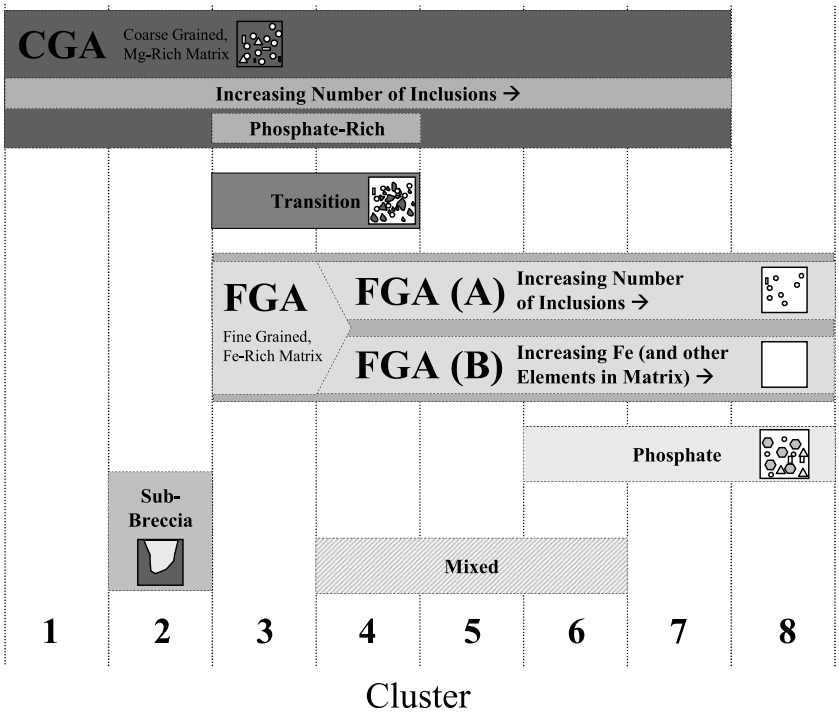

Fig. 8. Overview of the lithologies in CI chondrites, based on their basic mineralogical composition (groundmass, mineral inclusions) and hierarchical cluster analysis (vertical columns), which subdivides the lithologies. Clusters are ordered according to the increasing enrichment in several elements from 1 to 8. Cluster 8 is actually a group of outliers with high enrichments in some elements (e.g., P, Ca). For a more detailed description see text.

based on the clusters indicate trends in the contents of most elements from cluster 1–8. Iron, nickel, manganese, sulfur and sodium increase, while silicon, aluminum, and magnesium, consequently, decrease. The other elements show some variation, indicating their presence in rare phases.

This increase in the abundances of certain elements reflects an increasing abundance of inclusions or enrichment of elements in the groundmass of fragments—even fragments from the same lithology cover a wide range in composition. It is possible that the compositions of fragments actually cover a continuum, with the 'gaps', which divide the clusters, being the result of a bias in sample assortment.

Images of typical fragments of different lithologies are shown in Fig. 9a–j. The average chemistry and number of fragments of each lithology can be found in Table 2.

CGA lithology: The main characteristic of this lithology is a groundmass dominated by CGA, with varying abundances of mineral inclusions. Fragments representing the extreme end members of this lithology with low and high iron contents are shown in Figs. 1c and 9a–c. One group of CGA fragments contains phosphates (with wt% P_2O_5 of up to $\sim 3 \times$ CI).

Transition lithology: Fragments in this group consist of a FGA-rich groundmass, but they also have 'islands' of CGA within the groundmass (Fig. 9d). They may represent a transition stage between the CGA and FGA lithologies. This lithology is identical to lithology III of Endreß (1994) in Ivuna.

FGA lithologies: There are two distinct lithologies, both of which are characterized by FGA-rich groundmasses (Fig. 9e–h) and high iron contents (up to 42.4 wt% FeO; Table EA1). The first FGA lithology, FGA (A), has varying amounts of (usually small) mineral inclusions embedded in the groundmass (Fig. 9e and f); Fe, S, Mn, and Ni are enriched in these fragments. However, in fragments with a very high abundance of Fe in the groundmass, potential mineral inclusions such as magnetite are difficult to spot due to the small difference in contrast in the BSE images. This makes an exact classification difficult in some cases. The other FGA lithology, FGA (B), consists largely of groundmass material without many mineral inclusions (Fig. 1c and 9g, h). In addition to Fe, fragments of this lithology usually have high concentrations of S, Na, K, Mn, and Ni (Table 2). This lithology is identical to lithology IV of Endreß and Bischoff (1996), who found the majority of olivine grains observed in Ivuna to occur in this type of fragment.

Phosphate lithology: A second lithology has high contents of phosphates, in addition to the phosphate-rich CGA lithology. It contains a very high concentration of P_2O_5 up to $\sim 12 \times$ CI (Table 2). In addition, often very fine-grained phases, such as sulfides, sulfates, carbonates, magnetites, and Ti-rich minerals (Figs. 1a, b, and 9i) are present.

Sub-breccia: These fragments show relics of former brecciation cycles (Fig. 9j) and are basically fragments inside of fragments, for example, FGA-rich fragments surrounded by CGA-rich material.

Mixed lithologies: Fragments that do not fit into any other groups due to their heterogeneity are put into this group.

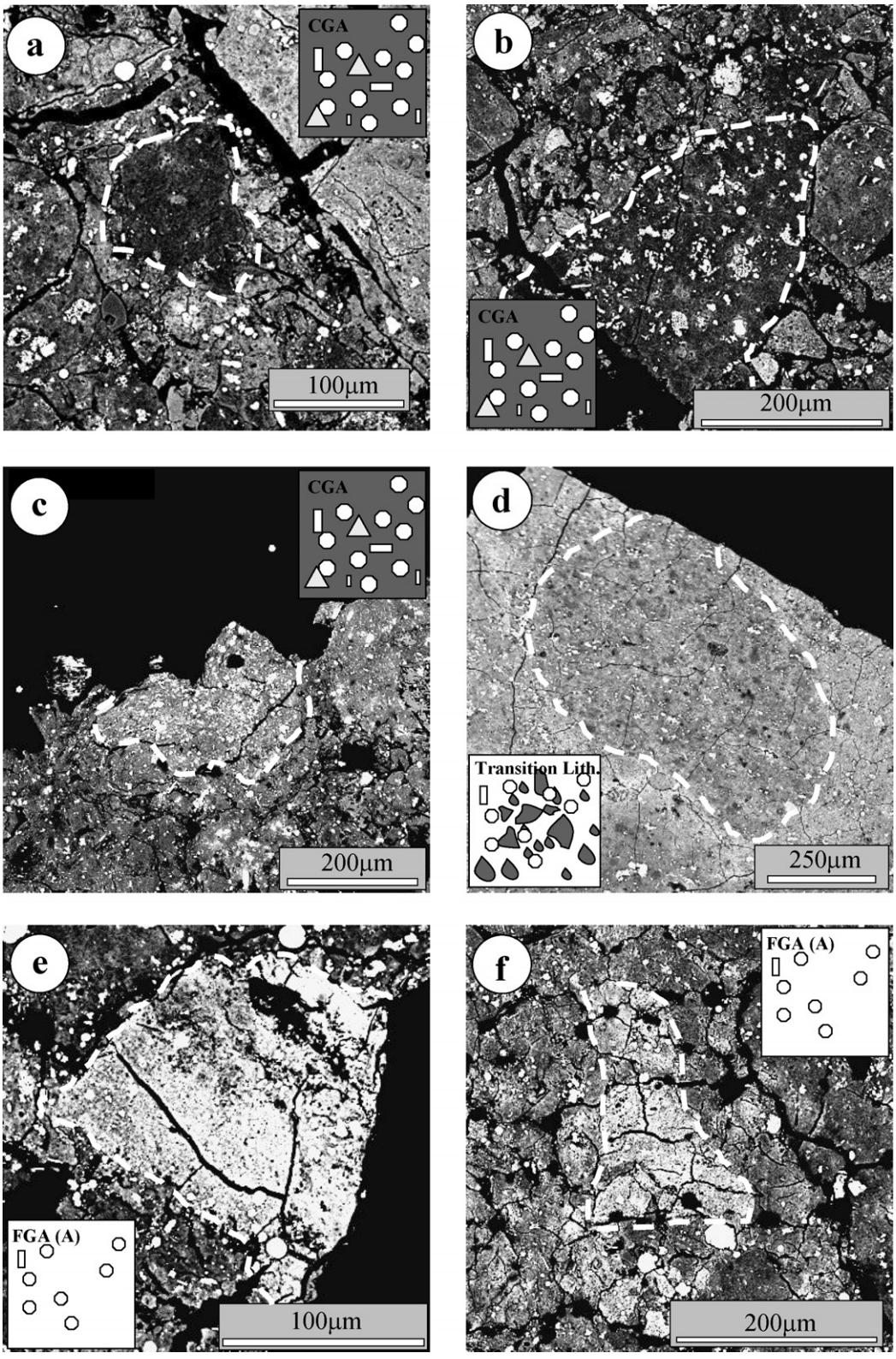

Fig. 9. (a–g) BSE images of representative fragments from the major lithologies in CI chondrites. The graphics are the same used in the diagrams modeling the proposed alteration process (Figs. 10 and 11). (a–c) Examples of fragments from the CGA lithology with increasing abundances of mineral inclusions in their groundmass, (c) a rare iron-rich end member of this lithology. (d) example of the transition lithology, with small 'islands' of CGA in a groundmass of iron-rich FGA material. (e), (f) Inclusion-rich FSA (A) lithology and (g, h) the groundmass-dominated FSA (B) lithology. (i) A sub-breccia with remnants of earlier brecciation cycles inside; in this case FGA fragments are surrounded by CGA material. (j) A phosphate-rich fragment. In addition to phosphates, these fragments also contain other mineral inclusions such as sulfides and sulfates.

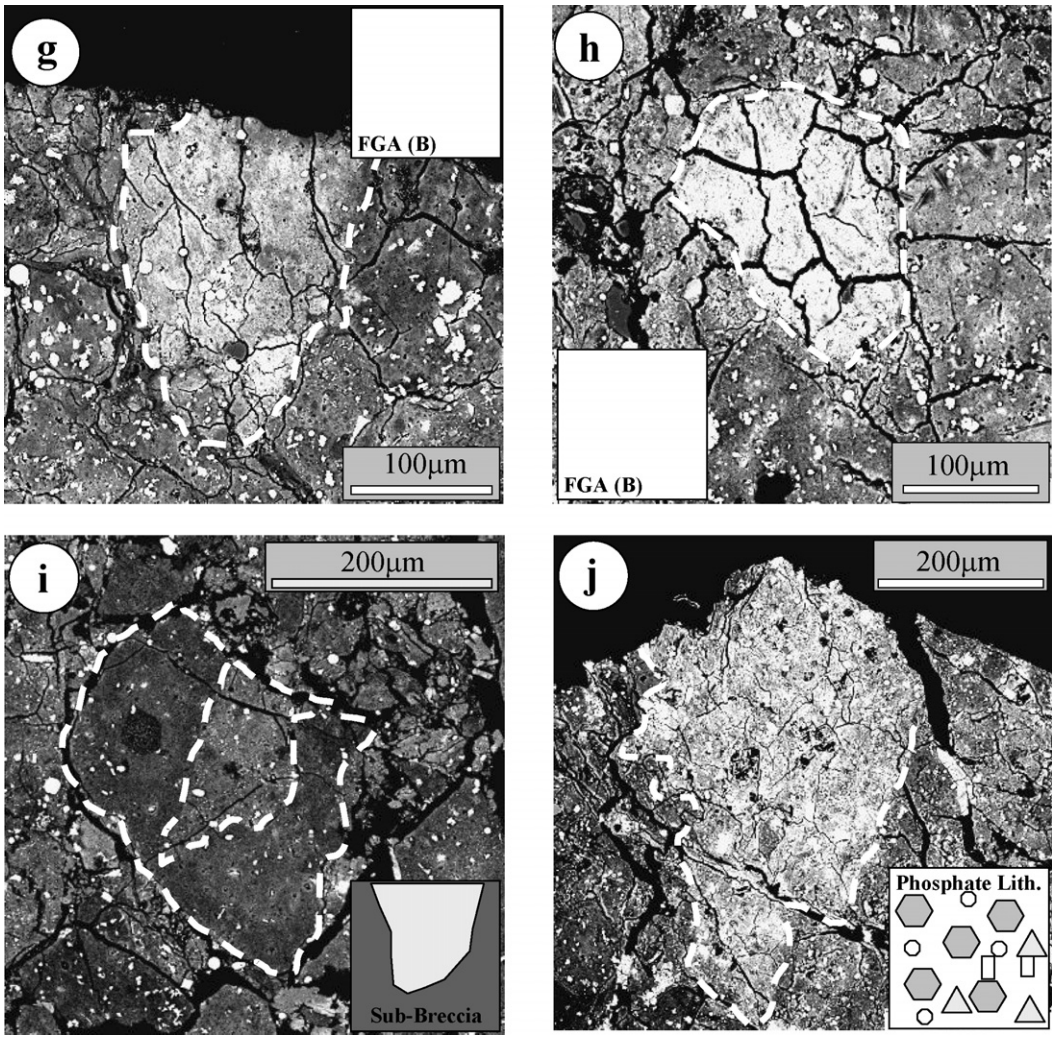

Fig. 9 (*continued*)

4.2.2. Formation of lithologies on the parent body

Based on analyses of Orgueil, Tomeoka and Buseck (1988) developed the first comprehensive model of the parent body alteration of CI chondrites. Endreß (1994) and Endreß and Bischoff (1996) combined this and several earlier studies (Richardson, 1978; McSween, 1987; Fredriksson and Kerridge, 1988; Tomeoka and Buseck, 1985, 1988; Tomeoka, 1990; Fisher and Burns, 1991; Buseck and Hua, 1993; Lee, 1993) into a more complex, but essentially similar model.

These models (Fig. 10) start with an early lithology of magnesium-rich phyllosilicates, carbonates, sulfides, and magnetite (Tomeoka and Buseck, 1988). This first lithology is probably represented by the CGA fragments.

The minerals of this first lithology were all attacked by fluid phases. The coarse-grained phyllosilicates degraded into fine-grained, poorly crystalized forms. Iron from dissolved magnetites and Fe(Ni) sulfides precipitated as ferrihydrites intergrown with the phyllosilicates (Tomeoka and Buseck, 1988). Experimental work by Jones and Brearley (2006) indicates that ferrous iron (Fe^{2+}) released by oxidation of sulfides is oxidized to ferric iron (Fe^{3+}) very quickly. This iron species is insoluble and tends to form iron oxide or oxyhydroxide phases closely associated with the source mineral.

Fragments from the transition lithology could be a 'snapshot' of this step. 'Islands' of magnesium-rich CGA groundmass would be the remains of the original materials, surrounded by altered, fine-grained, iron-rich FGA material.

An alternative formation mechanism of ferrihydrite has been suggested by Brearley and Prinz (1992), Zolensky et al. (1993), and Brearley (1997) in which ferrous iron in iron-rich saponite is oxidized, resulting in a breakdown into magnesium-rich saponite and ferrihydrite.

The FGA (A) lithology would be one of the last steps in this model. While the groundmass is converted to fine-grained, iron-rich material, remnants of the mineral inclusions are still left, but are dissolved by continuing alteration.

Increasing contents of sulfur and nickel, probably absorbed by ferrihydrite, indicate that the fluids were

Table 2
Average composition of lithologies

CGA	1	2	3	4	5	6	7	**Phosphate-rich**
Na_2O	0.30 ± 0.07	0.86 ± 0.49	0.89 ± 0.60	1.15 ± 0.69	1.10 ± 0.40	0.45	2.14	0.76 ± 0.45
Al_2O_3	3.86 ± 0.56	2.25 ± 0.16	2.13 ± 0.16	1.95 ± 0.15	1.95 ± 0.13	1.61	1.17	2.01 ± 0.19
MgO	25.20 ± 0.54	20.68 ± 1.39	19.76 ± 1.60	18.87 ± 0.87	16.86 ± 2.00	16.77	12.22	19.43 ± 1.24
SiO_2	41.17 ± 0.72	33.11 ± 2.36	31.55 ± 2.01	28.25 ± 1.88	26.05 ± 4.70	23.90	19.64	30.45 ± 2.50
SO_3	2.10 ± 1.25	6.68 ± 1.56	7.16 ± 2.34	7.99 ± 2.16	10.10 ± 3.30	4.73	10.29	6.23 ± 2.04
P_2O_5	0.05 ± 0.00	0.32 ± 0.32	0.19 ± 0.13	0.27 ± 0.17	0.14 ± 0.07	0.23	0.22	0.63 ± 0.23
K_2O	0.11 ± 0.05	0.12 ± 0.07	0.13 ± 0.05	0.15 ± 0.13	0.21 ± 0.06	0.10	0.10	0.14 ± 0.09
CaO	0.04 ± 0.01	0.59 ± 0.99	0.50 ± 0.77	0.83 ± 0.52	0.60 ± 0.09	0.64	0.26	1.19 ± 0.46
MnO	0.14 ± 0.02	0.19 ± 0.05	0.24 ± 0.12	0.21 ± 0.10	0.28 ± 0.07	0.08	0.31	0.18 ± 0.03
TiO_2	0.05 ± 0.00	0.07 ± 0.02	0.07 ± 0.01	0.06 ± 0.01	0.09 ± 0.01	0.08	0.06	0.07 ± 0.01
Cr_2O_3	0.39 ± 0.04	0.42 ± 0.08	0.41 ± 0.04	0.37 ± 0.09	0.37 ± 0.04	0.31	0.42	0.39 ± 0.06
FeO	11.58 ± 1.09	18.64 ± 1.47	20.89 ± 2.37	23.74 ± 0.70	25.55 ± 2.30	35.40	36.64	22.63 ± 2.49
NiO	0.37 ± 0.23	1.42 ± 0.25	1.45 ± 0.33	1.51 ± 0.69	2.05 ± 0.72	1.06	1.89	1.24 ± 0.17
Total	85.35 (4)	85.35 (20)	85.35 (28)	85.35 (9)	85.35 (2)	85.35 (1)	85.35 (1)	85.35 (5)

FGA (A)	4	5	6	7	8
Na_2O	1.10 ± 0.69	0.62 ± 0.11	0.65 ± 0.07	0.71	0.56
Al_2O_3	2.23 ± 0.39	1.76 ± 0.05	1.75 ± 0.50	1.48	0.98
MgO	16.49 ± 0.11	16.16 ± 0.75	12.53 ± 0.37	11.62	7.80
SiO_2	29.76 ± 2.51	25.80 ± 3.00	22.96 ± 3.23	20.58	14.21
SO_3	9.02 ± 2.09	10.79 ± 2.68	11.60 ± 3.92	11.80	15.76
P_2O_5	0.10 ± 0.03	0.21 ± 0.10	0.21 ± 0.07	0.11	0.36
K_2O	0.17 ± 0.11	0.20 ± 0.13	0.16 ± 0.11	0.06	0.12
CaO	0.13 ± 0.08	0.41 ± 0.43	1.06 ± 1.18	0.04	0.11
MnO	0.38 ± 0.12	0.30 ± 0.05	0.43 ± 0.14	0.56	0.29
TiO_2	0.09 ± 0.04	0.08 ± 0.01	0.10 ± 0.02	0.06	0.09
Cr_2O_3	0.42 ± 0.01	0.44 ± 0.03	0.50 ± 0.12	0.39	0.48
FeO	23.59 ± 0.17	26.74 ± 0.64	30.62 ± 1.35	35.92	42.44
NiO	1.89 ± 0.03	1.83 ± 0.22	2.77 ± 0.27	2.01	2.15
Total	85.35 (2)	85.35 (3)	85.35 (2)	85.35 (1)	85.35 (1)

FGA (B)	3	4	5	6	7	8
Na_2O	0.60	0.81 ± 0.27	1.23 ± 0.60	1.09 ± 0.74	1.04 ± 0.30	1.03
Al_2O_3	2.09	1.99 ± 0.11	1.90 ± 0.34	1.70 ± 0.16	1.19 ± 0.26	3.09
MgO	17.27	16.63 ± 0.42	14.99 ± 0.84	13.87 ± 1.05	11.88 ± 1.75	20.8
SiO_2	31.99	28.89 ± 1.42	27.42 ± 1.62	25.22 ± 1.72	18.05 ± 2.62	12.7
SO_3	7.57	9.48 ± 2.02	10.43 ± 1.73	9.24 ± 1.54	12.21 ± 2.04	14.8
P_2O_5	0.30	0.22 ± 0.10	0.22 ± 0.09	0.33 ± 0.09	0.28 ± 0.06	0.08
K_2O	0.26	0.25 ± 0.15	0.22 ± 0.14	0.24 ± 0.12	0.25 ± 0.12	0.09
CaO	0.08	0.30 ± 0.17	0.33 ± 0.72	0.28 ± 0.20	0.48 ± 0.53	0.06
MnO	0.37	0.24 ± 0.07	0.34 ± 0.13	0.27 ± 0.02	0.48 ± 0.24	0.60
TiO_2	0.07	0.07 ± 0.02	0.07 ± 0.02	0.10 ± 0.04	0.07 ± 0.02	0.08
Cr_2O_3	0.46	0.41 ± 0.03	0.46 ± 0.14	0.44 ± 0.08	0.35 ± 0.26	0.67
FeO	21.96	24.20 ± 0.96	25.58 ± 1.08	30.37 ± 2.00	36.67 ± 2.96	28.8
NiO	2.34	1.87 ± 0.27	2.17 ± 0.55	2.19 ± 0.30	2.38 ± 0.17	2.54
Total	85.35 (1)	85.35 (6)	85.35 (8)	85.35 (3)	85.35 (3)	85.35 (1)

	Phosphate lithology	**Sub-breccia**	**Transition lithology**	**Mixed lithology**
Na_2O	1.12 ± 0.41	0.56 ± 0.07	0.49 ± 0.08	0.66 ± 0.14
Al_2O_3	1.21 ± 0.29	2.22 ± 0.03	2.10 ± 0.09	2.01 ± 0.18
MgO	12.70 ± 1.54	20.63 ± 0.43	18.73 ± 1.04	16.22 ± 2.37
SiO_2	19.43 ± 3.40	35.65 ± 1.30	30.99 ± 1.21	27.89 ± 3.26
SO_3	9.82 ± 2.71	5.40 ± 0.68	8.58 ± 1.76	8.97 ± 3.24
P_2O_5	3.46 ± 2.40	0.19 ± 0.16	0.14 ± 0.08	0.15 ± 0.10
K_2O	0.06 ± 0.02	0.06 ± 0.01	0.29 ± 0.16	0.14 ± 0.09
CaO	4.29 ± 3.22	0.20 ± 0.24	0.18 ± 0.12	0.99 ± 1.29
MnO	0.37 ± 0.07	0.25 ± 0.08	0.20 ± 0.11	0.38 ± 0.08
TiO_2	0.10 ± 0.02	0.06 ± 0.00	0.08 ± 0.03	0.06 ± 0.01
Cr_2O_3	0.39 ± 0.03	0.46 ± 0.03	0.41 ± 0.02	0.44 ± 0.09
FeO	30.32 ± 2.74	18.30 ± 0.81	21.47 ± 0.83	25.58 ± 2.77
NiO	2.09 ± 0.04	1.39 ± 0.11	1.70 ± 0.17	1.86 ± 0.27
Total	85.35 (2)	85.35 (2)	85.35 (5)	85.35 (2)

EMPA data, normalized to solar system abundances (85.35 wt%). The numbers after the name of the lithology (bold) are the clusters from which the fragments come (for more details see Section 4). Number in bracket at bottom: number of fragments in the given lithology.

enriched in sulfur from dissolved sulfides of the earlier CGA lithologies (Kerridge, 1977; Tomeoka and Buseck, 1988). This also points to an overlap with the formation of sulfates, precipitating from sulfur-rich fluids (Tomeoka and Buseck, 1988; Endreß, 1994). Mobilization of volatile elements such as Na and K from an iron-rich FGA fragment into sulfates (Fig. 1d) also shows that leaching of elements may have continued throughout the alteration sequence.

Finally, in cases of complete alteration of the original material, fragments consisting only of an iron-rich, fine grained FGA groundmass are expected to be left. These would be represented by the FGA (B) lithology.

However, at least in Ivuna this lithology also contains the highest abundances of mafic olivine grains (Endreß and Bischoff, 1996), which would not be expected to occur in the lithology with the highest degree of alteration.

The remaining dissolved species left in the solutions, S, Ni, Ca, and Mg from dissolved carbonates and sulfides, formed carbonates and sulfates (Fig. 1e) (Richardson, 1978; Tomeoka and Buseck, 1988; Endreß and Bischoff, 1996).

This proposed alteration process remained obviously incomplete in most places on the parent body, as shown by the fact that fragments from different stages are still present, often in the same sample (Fig. 1c, 2, and 3). Relatively unaltered material was removed from the alteration process in one way or another early on, while alteration continued in other regions. Alternatively, the physical and chemical environment may have varied locally, to allow uneven alteration even on the small scale observed.

While there is some indication of exchange of volatile elements between fragments and matrix or veins (e.g., leaching of elements into sulfates, Fig. 1d), the boundaries between fragments and matrix are usually relatively sharp in the BSE and TOF-SIMS images, without reaction zones or rims. The range of chemical compositions for fragments of the same lithology (Table 2) is quite large, and is similar for both early (GSA) and late (FSA) formed lithologies.

This heterogeneity in chemical composition indicates that there was no complete equilibration of the material by physical or chemical processes on the parent body. While different degrees of alteration for the different CI chondrites have already been proposed (e.g., Brearley, 1997; Bullock et al., 2005), a closer look at fragments from the same samples indicates a wide range in alteration also within the same CI chondrites or even the same samples (e.g., Fig. 2). Tomeoka and Buseck (1988) also observed materials with different degrees of alteration in the same fragments of Orgueil.

This range in alteration points towards a very low mobility of materials in solution during aqueous alteration, probably on a scale of only 100 μm. However, not all elements show the same behavior in solution.

While, e.g., Fe^{3+} precipitates very fast, Ca^{2+}, K^{+}, Na^{+} or SO_4^{2-} are more mobile (Burger and Brearley, 2005; Jones and Brearley, 2006), which is also shown by the effective leaching of these components from the fragments and the formation of sulfates in veins. However, even these mobile elements probably precipitated close to where they were leached (Richardson, 1978; Endreß and Bischoff, 1996).

Recent models of the circulation of pore water on carbonaceous chondrite parent bodies suggest hydrothermal convection of the fluid phases in larger convection cells (Travis and Schubert, 2005; Zhang et al., 2005). This, however, does not result in complete homogenization: different parts of the body are affected by different convection cells. Furthermore, the degree of aqueous alteration varies in each convection cell.

Also, the limited mobilization of the materials as described above indicates that the homogenization even under such large-scale processes was limited.

In the following, we use the conclusions above to propose a tentative model (Fig. 11a and b). It is assumed, based on the findings above, that the mobility of all elements involved was low, thus we are dealing effectively with a closed system alteration. The ranges of Fe/Si-ratios for CGA and the FGA lithologies are similar. This indicates that each lithology in an earlier alteration stage has its 'equivalent' in later ones, representing a more altered version of the starting materials. Continuing alteration for an area with a given composition is represented by the horizontal lines in the figure.

Fragments of a lithology with, e.g., a low Fe/Si-ratio of ~1.5 would have evolved into transition lithology fragments, FGA (A) and, finally, FGA (B) fragments with a similar Fe/Si-ratio.

However, CGA fragments with very high and FGA lithologies with very low iron contents are missing, as well as most corresponding fragments for the transition lithology. Such fragments were not found in this study, but sampling bias could be responsible.

The picture is not as clear for other elements. Here the different behavior of elements in solution (combined with changes in the physical environment) may play a role.

4.2.3. Phosphate lithology

The origin of phosphates in CI chondrites has been neglected so far, despite their importance as a 'sink' for trace elements such as the REE. Studies of alteration in CM2 and CR2 chondrites may provide information about the origins of the phosphate lithology. Brearley and Chizmadia (2005) and Burger and Brearley (2005) observed the formation of Ca-phosphate at the boundary regions between chondrule mesostasis and surrounding fine-grained rim and matrix material. There is, so far, no documentation of the evolution of such phases during later stages of parent body alteration. An analogous alteration of (hypothetical) chondrules in the precursor materials of CI chondrites could mean that the rare phosphate-rich fragments are late remnants of these components.

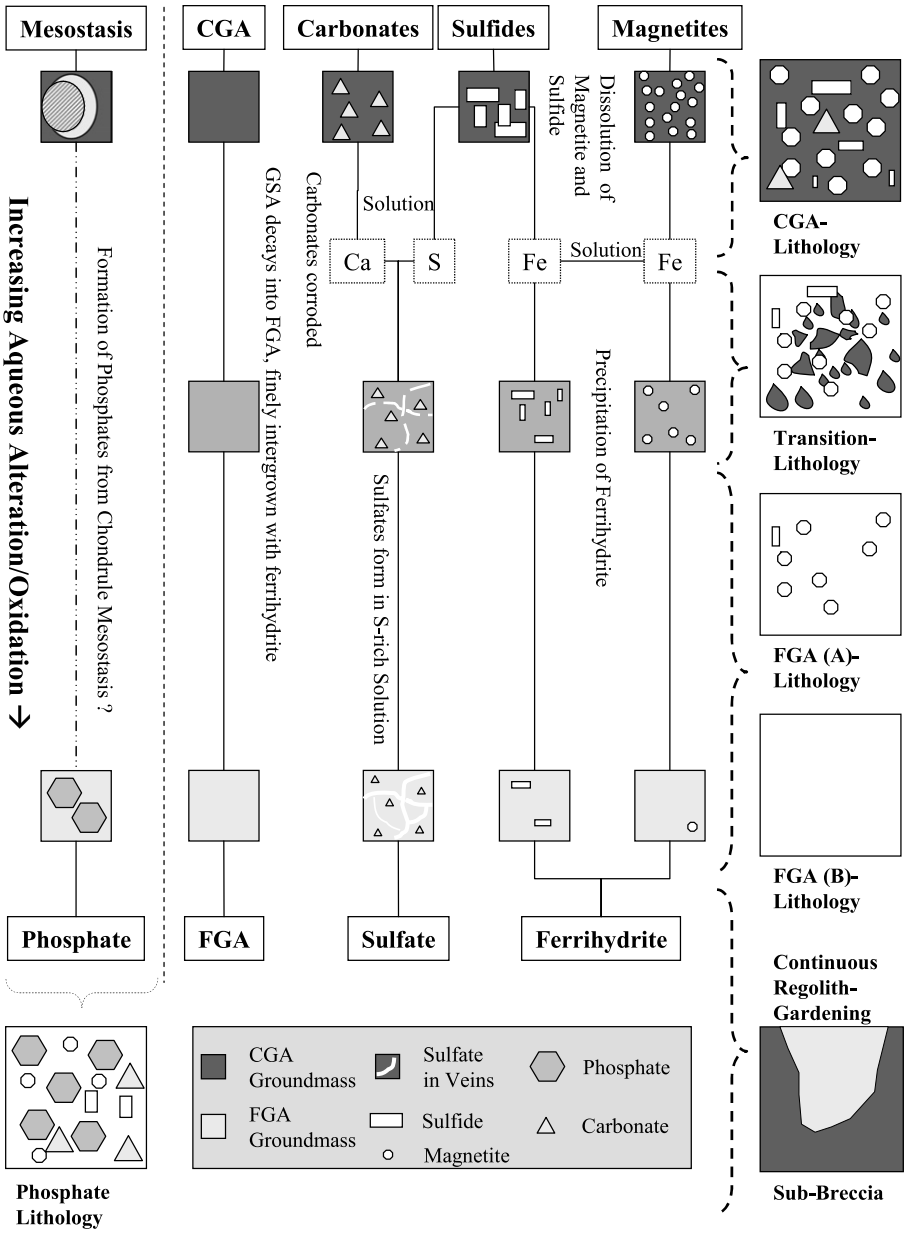

Fig. 10. Schematic overview of the late-stage aqueous alteration of the CI chondrite parent body (compiled from Richardson, 1978; McSween, 1987; Tomeoka and Buseck, 1985, 1988; Fredriksson and Kerridge, 1988; Fisher and Burns, 1991; Buseck and Hua, 1993; Lee, 1993; Endreß, 1994). The most important development is the evolution of the coarse-grained phyllosilicates into fine-grained material. In addition, carbonates and sulfides from the starting lithology dissolve, while sulfates are formed. Iron hydroxides (possibly ferrihydrite) form from the iron-rich component of dissolved sulfides and magnetites. The different lithologies observed in this study may represent several stages of this model. The CGA lithology, dominated by magnesium-rich, coarse grained phyllosilicates and magnetites, carbonates, and sulfides would be equivalent to the original composition. The FGA (A) lithology, basically consisting of an iron-rich, fine-grained matrix with varying abundances of inclusions, could be representative of a later stage of alteration, with the FGA (B) fragments, basically only consisting of matrix, representing the final late-stage end members. For more details see text.

4.3. Distribution of lithologies in CI chondrites and chemical heterogeneity of CI chondrites as result of alteration and brecciation?

A central question in connection with the occurrence of specific lithologies in the CI chondrites is whether they are responsible for chemical heterogeneity on a larger scale.

Any conclusion about the parent body of CI chondrites in connection with the fragments is based on the assumption that the fragments actually represent the whole meteorite. However, the fragments are embedded in matrix material, which also has to be accounted for. Given that there is no actual lower size limit for fragments—they seem to blend into the matrix at the lower end of the size scale—we think that matrix and fragments basically represent the same material. We also have to be aware of secondary minerals such as sulfates and carbonates (McSween and Richardson, 1977; Gounelle and Zolensky,

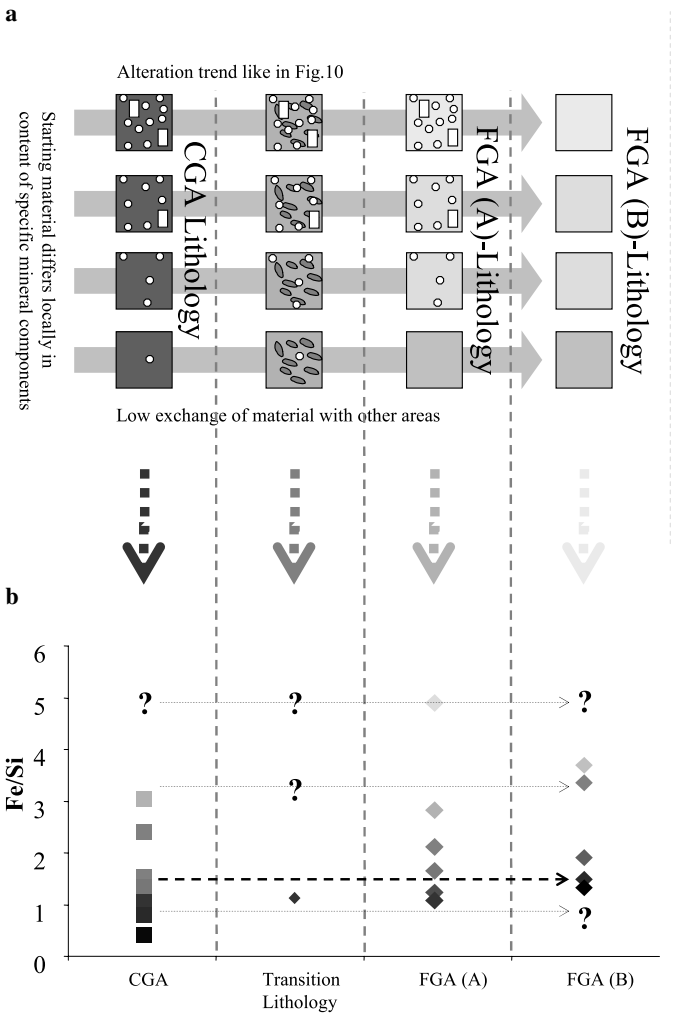

Fig. 11. (a, b): A proposed model that correlates the various types of lithologies with the aqueous alteration of the CI chondrites (Fig. 10). (a) Without transport of significant amounts of material over larger distances (e.g., Endreß, 1994), the composition of the starting material determines the mineralogy of the final lithology. Each row represents a region with different mineralogical and thus chemical composition. The arrows indicate the aqueous alteration trend according to the model in Fig. 10 for a specific region, where CGA lithologies are altered into FGA-B lithologies with some intermediate steps. (b) An attempt is made to correlate the actual lithologies observed in this study with the model in (a), based on their Fe/Si ratio. Here, the sub-lithologies of the specific lithologies remain for the 'individual' local evolution trends, depending on the starting composition. While there is a wide range of compositions for the CGA and FGA lithologies, there is clearly a lack of corresponding fragments for the transition lithology, and extreme end members for the other lithologies, as indicated by the question marks. This could be a result of sample bias, or could point to the effect of additional evolutionary trends.

2001), which represent a further source of heterogeneity not directly addressed here.

All of the observed lithologies are found in Orgueil, but in Ivuna some were missing, and Alais and Tonk appear to contain only a limited number of lithologies. However, this difference could be a result of sample bias. To obtain a more comprehensive picture, the compositions of matrix material and phyllosilicates from the literature for Orgueil, Ivuna, and Alais (Fig. 7a and b) were compared in ternary diagrams. The data from our fragments fall into the regions defined for Orgueil, Ivuna, and Alais, indicating the similarity of fragments with matrix material from these studies. This is supported by the fact that only a few fragments with high iron contents from this study lie outside of these areas. Compared with each other, matrix material and phyllosilicates from the literature show similar ranges of composition in Orgueil, Ivuna and Alais. Here it is important to keep in mind that the lithologies are mainly characterized by the composition of their groundmass. So while it may not be possible to directly identify the various lithologies from the ternary diagrams, we can still infer the general distributions of the basic types of fragments from the ternary diagrams. While it is not possible to make any quantitative estimate of the distribution of these components (and accordingly, of the fragment types) among the different CI chondrites, they do seem to be similar with regard to the range in composition.

This homogeneity could also indicate that the various CI chondrites represent, if not identical, at least similar source materials, and that the observed differences are merely the result of varying abundances of specific lithologies. It could, thus, also indicate that the actual heterogeneity in CI chondrites lies not necessarily at the level of the different meteorites, but at the size scale of fragments.

4.4. Impact of mineralogical heterogeneities on bulk compositions of CI chondrites

One way to assess the influence of fragment distributions on the chemical homogeneity of the CI chondrites is to compare the ranges of concentrations of specific elements among the fragments with those of bulk analyses of CI chondrites from the literature made since 1970. Bulk analyses should exhibit a much narrower range than analyses of fragments (Fig. 12). This is, indeed, the case for all presented elements; most of the CI-normalized elements have more than twice the range in the fragments than in the bulk analyses. Only for iron, sulfur, calcium, manganese, and chromium the range in fragments is less than twice the bulk range.

In addition, when outliers are excluded, the range in composition for the majority of fragments (as represented by the 50% boxes in the boxplots) is also more than twice that for bulk measurements. Exceptions are calcium and chromium, where the differences in range are smaller.

However, while most bulk ratios cluster around or close to the solar composition, there are some extreme outliers that diverge strongly from CI. In bulk analyses, calcium can be enriched up to three times the solar abundance, followed by manganese ($2.5 \times$ CI). Manganese also can be strongly depleted ($0.3 \times$ CI), like sodium, sulfur, chromium, and iron (down to $0.4 \times$ CI). The situation for minor and trace elements is similar; see the extensive data sets in Anders and Ebihara (1982) and Anders and Grevesse (1989). However, the

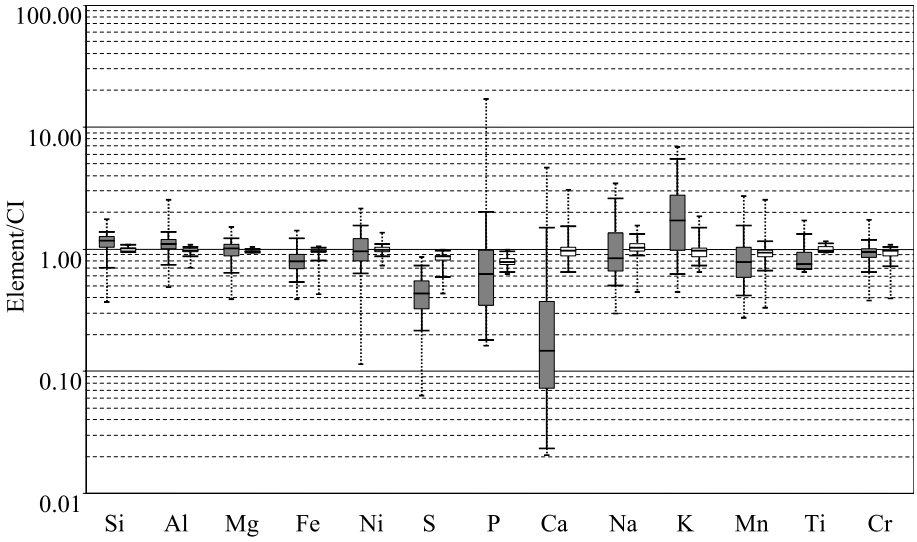

Fig. 12. Ranges in composition for fragments (right, dark boxplots) and bulk analyses from the literature since 1970 (left boxplot). Data are normalized to CI, and presented as boxplots (see Fig. 4 for details). The fragments show a wider range in composition than the bulk measurements. The reason for this variability is that the mineralogical differences among the various types of fragments is much larger than those of the to bulk materials, which are the average of various types of fragments. Most data are from the comprehensive compilations in Nagy (1975), Anders and Ebihara (1982) and Anders and Grevesse (1989). Additional data are from Nichiporuk and Moore (1970), Mason (1971), Ehmann and Gillum (1972), Fisher (1972), De Laeter et al. (1974), Ehmann and Chyi (1974), Grossman and Ganapathy (1976), De Laeter and Hosie (1978), Dreibus et al. (1979), Kiesl (1979), Ganapathy and Larimer (1980), Jarosewich (1990), Baars et al. (1993); Endreß (1994); Gao and Thiemens (1993), Rocholl and Jochum (1993), Spettel et al. (1993), Dreibus et al. (1995), Wolf and Palme (1997) and Friedrich et al. (2002).

significance of the extreme values remains unclear. Are they merely outliers, due to contamination or heterogeneities, or should these extremes be taken into account for representative bulk analyses of this type of meteorite ? Could these outliers reflect larger-scale heterogeneity as result of varying types of lithologies and possibly secondary phases? It should be noted that these literature data are a compilation of analyses based on various analytical methods and, therefore, may in some cases be subject to systematic biases.

In the widely used solar system abundances of the elements by Anders and Ebihara (1982) and Anders and Grevesse (1989), cosmic abundances for certain elements are obtained by averaging the results of earlier analyses of (mostly) CI chondrites. Values thought to be outliers are sometimes rejected, assuming that they are the result of contamination, non-typical components like CAI, or technical difficulties. While all these factors certainly can be responsible for some outliers, mineralogical and, thus, chemical heterogeneities in different types of fragments may also have led to some of these extreme concentrations. Thus, for example, outliers of REE and P could be the result of concentrations or depletions of phosphate-rich fragments.

Another possible source of chemical heterogeneity is the sample size or mass analyzed, as already indicated by comparison of fragments and bulk measurements. Bulk analyses reported in the literature were made on samples ranging from below 0.01 g up to 5.5 g. Small samples could be easily affected by heterogeneities due to the presence of fragments even far below sub-mm-scale. When averaged divergences of bulk measurements from CI are compared with the analyzed amount of material (Fig. 13), most divergences larger than ±50% occur for analyses with less than ~1–2 g mass analyzed. This amount could indicate a minimum mass of material needed for representative chemical analyses. Given an average density of CI chondrites of 2.23 g/cm^3 (Lodders and Fegley, 1998), 1 g of CI chondrite corresponds to a volume of 0.45 cm^3, equivalent to 150 cm^2 of a thin section with a thickness of 30 μm. Depending on the 'information depth' of specific analytical technologies, it would be necessary to analyze even larger amounts of sample to get a representative picture of the composition of CI chondrites.

For electron microprobe techniques, where material is analyzed down to ~5 μm below the sample surface, the area would increase to 900 cm^2. For surface sensitive techniques such as TOF-SIMS, where only a monolayer on the surface is sputtered, the area would be many orders of magnitude larger (4.5×10^6 cm^2).

5. Conclusions and outlook

Fragments in the CI chondrites Orgueil, Ivuna, Alais, and Tonk show a wide range of chemical compositions. Major elements such as iron and sulfur, but also important trace elements such as the REE have variable abundances. This is the result of the different mineralogical compositions of these fragments, mainly the distribution of phyllosilicates, iron-bearing phases such as magnetite and ferrihydrite, sulfates, and phosphates.

The fragments have been classified into groups or lithologies with similar mineralogical and, thus, chemical

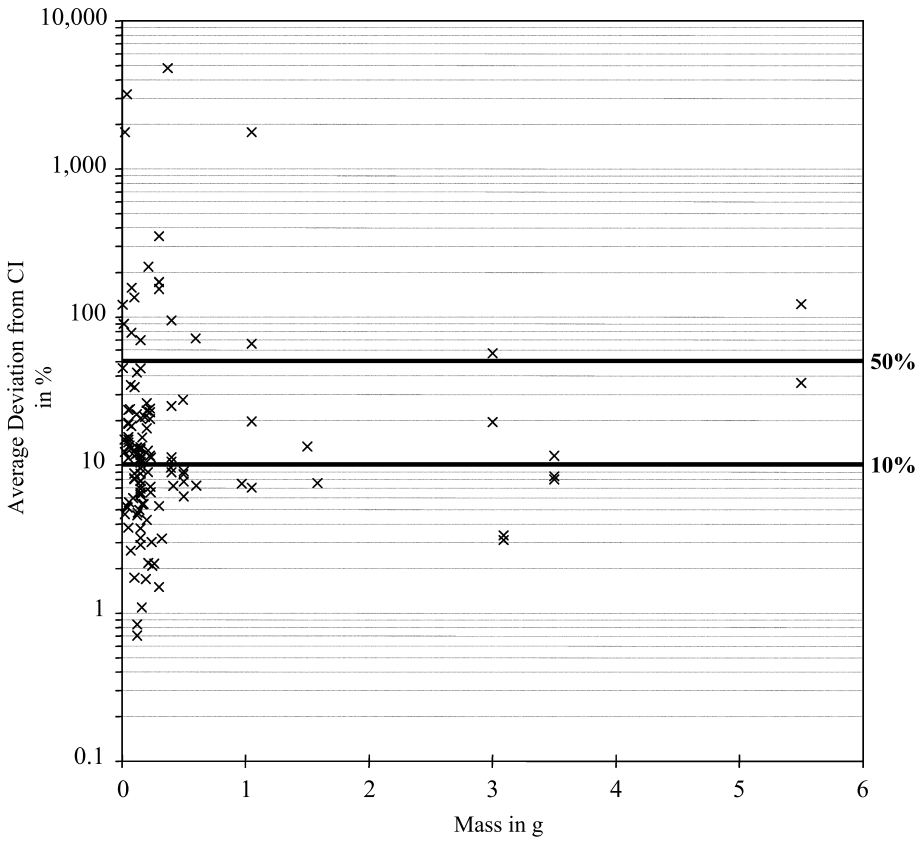

Fig. 13. Average divergence (in %) of bulk CI analyses vs. the mass of sample analyzed. Here, all divergences from CI of elements in a given study were averaged. The horizontal lines show 50% and 100% divergence from CI. The largest deviations are found for sample sizes below ~1–2 g. Literature data are from the same sources (if information about sample mass analyzed was given) as in Fig. 12.

properties. The dominant lithologies are the CGA lithology, comprising fragments consisting of a groundmass of Mg-rich, coarse-grained phyllosilicates and varying contents of inclusions (mostly magnetites), and the FGA lithology in which the groundmass is composed of fine-grained Fe-rich phyllosilicates. A rare, but important lithology contains fragments with high contents of phosphates.

A simple model explains the formation of these lithologies in a system where most mineralogical differences of the lithologies reflect heterogeneity of the starting material.

There is an indication for a similarity of these meteorites with regard to the major lithologies. Further comparison of bulk analyses also suggests that the mass 'threshold' for chemical heterogeneities in CI chondrites is in samples of less than ~1–2 g mass.

Since the widely used data for solar system abundances are based on results from analyses of varying amounts of material and different techniques (Anders and Grevesse, 1989; Lodders, 2003), a systematic analysis of larger amounts (more than 1–2 g) of unaltered samples of CI chondrites (especially with regard to the terrestrial formation of sulfates) is recommended.

Acknowledgments

We thank Thorsten Grund and Michael Enders for electron microprobe and SEM assistance, Torsten Henkel (Manchester) and Detlef Rost (Washington) for TOF-SIMS support. Thanks are also due to Associate Editor S. Krot, as well as G. Huss and two anonymous reviewers. We are grateful to Caroline Smith (London) and Emma Bullock (Washington) for proofreading the early manuscript, and to Iris and Dietmar Weber (Münster) for additional help. This work is based on the Ph.D. thesis of A.M. at the Institut für Planetologie in Münster, and was mainly supported by the Graduiertenkolleg "Entstehung und Entwicklung des Sonnensystems" of the Deutsche Forschungsgemeinschaft (DFG).

Associate editor: Alexander N. Krot

Appendix A. Supplementary data

Supplementary data associated with this article can be found, in the online version, at doi:10.1016/j.gca.2006.08.007.

References

Alexander, C.M.O'D., 1994. Trace element distributions within ordinary chondrite chondrules: Implications for chondrule formation conditions and precursors. *Geochim. Cosmochim. Acta* **58**, 3451–3467.

Anders, E., Ebihara, M., 1982. Solar system abundances of the elements. *Geochim. Cosmochim. Acta* **46**, 2363–2380.

Anders, E., Grevesse, N., 1989. Abundances of the elements: meteoritic and solar. *Geochim. Cosmochim. Acta* **53**, 197–214.

Baars, J.W., Beer, H., Durrant, C.J., Graser, U., Guinot, B., Hoffmann, M., Hopp, U., Ip, W.-H., Jessberger, E.K., Klecker, B., Lemke, D., Meisenheimer, K., Möbius, E., Palme, H., Rahe, J., Röser, H.J., Schubart, J., Schwenn, R., Solf, J., Soltau, G., Staubert, R., Stewart, R., Trümper, J., Vanysek, V., Weigelt, G., Wolf, R., 1993. Extension and supplement to volume 2 instruments, methods, Solar System, XVIII. In: Voigt, H.H. (Ed.), *Landolt-Börnstein: New Series Gruppe/ Group 6 Astronomy and Astrophysics Volume 3: Astronomy and Astrophysics*. Springer-Verlag, Berlin Heidelberg New York, p. 221.

Bischoff, A., Schultz, L., 2004. Abundance and meaning of regolith breccias among meteorites. *Meteor. Planet. Sci.* **39**, A15 (Abstract).

Bischoff, A., Scott, E.R.D., Metzler, K., Goodrich, C.A., 2006. Nature and origins of meteoritic breccias. In: Lauretta, D.S., McSween, H.Y., Jr.Jr. (Eds.), *Meteorites and the Early Solar System II*. Univ. of Arizona, Tucson, pp. 679–712.

Bland, P.A., Cressey, G., Menzies, O.N., 2004. Modal mineralogy of carbonaceous chondrites by X-ray diffraction and Mössbauer spectroscopy. *Meteorit. Planet. Sci.* **39**, 3–16.

Boström, K., Fredriksson, K., 1966. Surface conditions of the Orgueil parent meteorite body as indicated by mineral associations. *Smithsonian Misc. Coll.* **151** (3), 39 pp..

Brearley, A.J., 1992. Mineralogy of fine-grained matrix in the Ivuna CI carbonaceous chondrite*Lunar Planet. Sci.*, vol. XXIII. Lunar Planet. Inst., Houston, pp. 153–154 (Abstract).

Brearley, A.J., 1997. Phyllosilicates in the matrix of the unique carbonaceous chondrite Lewis Cliff 85332, and possible implications for the aqueous alteration of CI chondrites. *Meteorit. Planet. Sci.* **32**, 377–388.

Brearley, A.J., Chizmadia, L.J., 2005. On the behavior of phosphorus during the aqueous alteration of CM2 carbonaceous chondrites*Lunar Planet. Sci.*, vol. XXXVI. Lunar Planet. Inst., Houston, #2176 (Abstract).

Brearley, A.J., Jones, R.H., 1998. Chondritic meteorites. In: Papike, J.J. (Ed.), *Reviews in Mineralogy 36: Planetary Materials*. Mineralogical Society of America, Washington, DC, pp. 3-01–3-398.

Brearley, A.J., Prinz, M., 1992. CI chondrite-like clasts in the Nilpena polymict ureilite: Implications for aqueous alteration processes in CI chondrites. *Geochim. Cosmochim. Acta* **56**, 1373–1386.

Brookins, D.G., 1989. Aqueous geochemistry of rare earth elements. In: Lipin, B.R., McKay, G.A. (Eds.), *Reviews in Mineralogy*, *Rare Earth Elements*, vol. 21. Mineralogical Society of America, Washington, DC.

Bullock, E.S., Gounelle, M., Lauretta, D.S., Grady, M.M., Russell, S.S., 2005. Mineralogy and texture of Fe–Ni sulfides in CI1 chondrites: Clues to the extent of aqueous alteration on the CI1 parent body. *Geochim. Cosmochim. Acta* **69**, 2687–2700.

Burger, P.V., Brearley, A.J., 2005. Localized chemical redistribution during aqueous alteration in CR2 carbonaceous chondrites EET 87770 and EET 92105*Lunar Planet. Sci.*, vol. XXXVI. Lunar Planet. Inst., Houston, #2288 (Abstract).

Burgess, R., Wright, I.P., Pillinger, C.T., 1991. Determination of sulphur-bearing components in C1 and C2 carbonaceous chondrites by stepped combustion. *Meteoritics* **26**, 55–64.

Buseck, P.R., Hua, X., 1993. Matrices of carbonaceous chondrite meteorites. *Annu. Rev. Earth Planet. Sci.* **21**, 255–305.

Crozaz, G., Pellas, P., Bourot-Denise, M., de Chazal, S.M., Fiéni, C., Lundberg, L.L., Zinner, E., 1989. Plutonium, uranium and rare earths in the phosphates of ordinary chondrites – the quest for a chronometer. *Earth Planet. Sci. Lett.* **93**, 157–169.

De Laeter, J.R., Hosie, D.J., 1978. The abundance of barium in stony meteorites. *Earth Planet. Sci. Lett.* **38**, 416–420.

De Laeter, J.R., McCulloch, M.T., Rosman, K.J.R., 1974. Mass spectrometric isotope dilution analyses of tin in stony meteorites and standard rocks. *Earth Planet. Sci. Lett.* **22**, 226–232.

Dreibus, G., Spettel, B., Wänke, H., 1979. Halogens in meteorites and their primordial abundances. In: Ahrens, C.H. (Ed.), *Origin and Distribution of Elements*. Pergamon Press, New York, pp. 33–38.

Dreibus, G., Palme, H., Spettel, B., Zipfel, J., Wänke, H., 1995. Sulfur and selenium in chondritic meteorites. *Meteoritics* **30**, 439–445.

Ehmann, W.D., Chyi, L.L., 1974. Zirconium and hafnium in meteorites. *Earth Planet. Sci. Lett.* **21**, 230–234.

Ehmann, W.D., Gillum, D.E., 1972. Platinum and gold in chondritic meteorites. *Chem. Geol.* **9**, 1–11.

Endreß, M., 1994. Mineralogische und chemische Untersuchungen an CI-Chondriten – Ein Modell zur mineralogisch-kosmochemischen Evolution der(s) CI-Mutterkörper(s). Ph.D. Thesis, University of Muenster.

Endreß, M., Bischoff, A., 1994. Carbonates in the CI-chondrite Ivuna: Implications for aqueous alteration processes on the CI-parent body*Lunar Planet. Sci.*, vol. XXV. Lunar Planet. Inst., Houston, pp. 349–350 (Abstract).

Endreß, M., Bischoff, A., 1996. Carbonates in CI chondrites: clues to parent body evolution. *Geochim. Cosmochim. Acta* **60**, 489–507.

Endreß, M., Zinner, E., Bischoff, A., 1996. Early aqueous activity on primitive meteorite parent bodies. *Science* **379**, 701–703.

Evensen, N.M., Hamilton, P.J., O'Nions, R.K., 1978. Rare-earth abundances in chondritic meteorites. *Geochim. Cosmochim. Acta* **42**, 1199–1212.

Fisher, E.F., 1972. Uranium content and radiogenic ages of hypersthene, bronzite, amphoterite and carbonaceous meteorites. *Geochim. Cosmochim. Acta* **36**, 15–33.

Fisher, D.S., Burns, R.G., 1991. Pre-terrestrial oxidation products of iron minerals in carbonaceous chondrites identified in Mössbauer spectra*Lunar Planet. Sci.*, vol. XXII. Lunar Planet. Inst., Houston, pp. 389–390 (Abstract).

Fredriksson, K., Kerridge, J.F., 1988. Carbonates and sulfates in CI chondrites: formation by aqueous activity on the parent body. *Meteoritics* **23**, 35–44.

Friedrich, J.M., Wang, M.-S., Lipschutz, M.E., 2002. Comparison of the trace element composition of Tagish Lake with other primitive carbonaceous chondrites. *Meteorit. Planet. Sci.* **37**, 677–686.

Ganapathy, R., Larimer, J.W., 1980. A meteoritic component rich in volatile elements: Its characterization and implications. *Science* **207**, 57–59.

Gao, X., Thiemens, M.H., 1993. Isotopic composition and concentration of sulfur in carbonaceous chondrites. *Geochim. Cosmochim. Acta* **57**, 3159–3169.

Gounelle, M., Zolensky, M.E., 2001. A terrestrial origin for sulfate veins in CI1 chondrites. *Meteorit. Planet. Sci.* **36**, 1321–1329.

Grossman, L., Ganapathy, R., 1976. Trace elements in the Allende meteorite – I. Coarse-grained, Ca-rich inclusions. *Geochim. Cosmochim. Acta* **40**, 331–344.

Hua, X., Wang, J., Buseck, P.R., 2002. Fine-grained rims in the Allan Hills 81002 and Lewis Cliff 90500 CM2 meteorites: their origin and modification. *Meteorit. Planet. Sci.* **37**, 229–244.

Jarosewich, E., 1990. Chemical analyses of meteorites: a compilation of stony and iron meteorite analyses. *Meteoritics* **25**, 323–337.

Jones, C.L., Brearley, A.J., 2006. Experimental aqueous alteration of the Allende meteorite under oxidizing conditions: constraints on asteroidal alteration. *Geochim. Cosmochim. Acta* **70**, 1040–1058.

Kerridge, J.F., 1967. The mineralogy and genesis of the carbonaceous chondrites. In: Runcorn, S.K. (Ed.), *Mantles of the Earth and Terrestrial Planets*. Interscience Publishers, London and New York, pp. 35–47.

Kerridge, J.F., 1976. Major element composition of phyllosilicates in the Orgueil carbonaceous meteorite. *Earth Planet. Sci. Lett.* **29**, 194–200.

Kerridge, J.F., 1977. Correlation between nickel and sulfur abundances in Orgueil phyllosilicates. *Geochim. Cosmochim. Acta* **41**, 1163–1164.

Kiesl, W., 1979. *Kosmochemie*. Springer-Verlag, Wien and New York.

Lee, M.R., 1993. The petrography, mineralogy and origins of calcium sulphate within the Cold Bokkefeld CM carbonaceous chondrite. *Meteoritics* **28**, 53–62.

Lodders, K., 2003. Solar system abundances and condensation temperatures of the elements. *Astrophys. J.* **591-2**, 1220–1247.

Lodders, K., Fegley Jr., B., 1998. *The Planetary Scientist's Companion*. Oxford University Press, New York, 371 pp..

MacKinnon, I.D.R., Kaser, S.A., 1988. Trace phases in CI chondrites Alais and Orgueil. *Meteoritics* **25**, 381–382.

Madsen, M.B., Morup, S., Costa, T.V.V., Knudsen, J.M., Olsen, M., 1986. Superparamagnetic component in the Orgueil meteorite and Moessbauer spectroscopy studies in applied magnetic fields. *Nature* **321**, 501–503.

Mason, B., 1971. *Handbook of Elemental Abundances in Meteorites*. Gordon and Breach Science Publishers.

McSween Jr., H.Y., 1987. Aqueous alteration in carbonaceous chondrites: mass balance constraints on matrix mineralogy. *Geochim. Cosmochim. Acta* **51**, 2469–2477.

McSween Jr., H.Y., Richardson, S.M., 1977. The composition of carbonaceous chondrite matrix. *Geochim. Cosmochim. Acta* **41**, 1145–1161.

Morlok, A., Bischoff, A., Henkel, T., Rost, D., Stephan, T., Jessberger, E.K., 2001. Chemical variation in CI chondrites: degree and implications. *Meteorit. Planet. Sci.* **36**, A141 (Abstract).

Mueller, G., Bernal, J.D., 1966. Significance of inclusions in carbonaceous meteorites. *Nature* **210**, 151–155.

Nagy, B., 1975. *Carbonaceous Chondrites*. Elsevier, Amsterdam.

Nichiporuk, W., Moore, C.B., 1970. Lithium in chondritic meteorites. *Earth Planet. Sci. Lett.* **9**, 280–286.

Richardson, S.M., 1978. Vein formation in the C1 carbonaceous chondrite. *Meteoritics* **13**, 141–159.

Rocholl, A., Jochum, K.P., 1993. Th, U and other trace elements in carbonaceous chondrites – implications for the terrestrial and solar-system Th/U ratios. *Earth Planet. Sci. Lett.* **117**, 265–278.

Rollinson, H., 1993. *Using Geochemical Data*. Longman, Essex.

Spettel, B., Palme, H., Dreibus, G., Wänke, H., 1993. New analyses of CI chondrites: refinement of solar system abundances. *Meteorit. Planet. Sci.* **28**, 440 (Abstract).

Stephan, T., 2001. TOF-SIMS in cosmochemistry. *Planetary and Space Science* **49**, 859–906.

Tomeoka, K., 1990. Matrix compositions and mineralogy of the Alais and Ivuna CI carbonaceous chondrites*Lunar Planet. Sci.*, vol. XXI. Lunar Planet. Inst., Houston, pp. 1256–1257 (Abstract).

Tomeoka, K., Buseck, P., 1985. Indicators of aqueous alteration in CM carbonaceous chondrites: microtextures of a layered mineral containing Fe, S, O and Ni. *Geochim. Cosmochim. Acta* **49**, 2149–2163.

Tomeoka, K., Buseck, P., 1988. Matrix mineralogy of the Orgueil CI carbonaceous chondrite. *Geochim. Cosmochim. Acta* **52**, 1627–1640.

Travis, B.J., Schubert, G., 2005. Hydrothermal convection in carbonaceous chondrite parent bodies. *Earth Planet. Sci. Lett.* **240**, 234–250.

Wdowiak, T.J., Agresti, D.G., 1984. Presence of a superparamagnetic component in the Orgueil meteorite. *Nature* **311**, 140–142.

Wernecke, K.-D., 1995. *Angewandte Statistik für die Praxis*. Addison-Wesley, Bonn and Paris.

Wolf, D., Palme, H., 1997. A revision of the solar system phosphorous abundance. *Meteorit. Planet. Sci.* **32**, 4 (Abstract).

Zhang, K., Liao, X., Schubert, G., 2005. Pore water convection within carbonaceous chondrite parent bodies: temperature-dependent viscosity and flow structure. *Phys. Fluids* **17**, 086602-1–086602-12.

Zinner, E., Crozaz, G., 1986. A method for the quantitative measurement of rare earth elements in the ion microprobe. *Int. J. Mass Spectrom. Ion Process.* **69**, 17–38.

Zolensky, M.E., Barrett, R.A., Gooding, J.L., 1989. Matrix and rim compositions compared for 13 carbonaceous chondrite meteorites and clasts*Lunar Planet. Sci.*, vol. XX. Lunar Planet. Inst., Houston, pp. 1249–1250 (Abstract).

Zolensky, M.E., Barrett, R., Browning, L., 1993. Mineralogy and composition of matrix and chondrule rims in carbonaceous chondrites. *Geochim. Cosmochim. Acta* **57**, 3123–3148.